The Pennsylvania State University

The Graduate School

Department of Materials Science and Engineering

COMPUTER SIMULATIONS OF FERROELECTRIC LOCAL SWITCHING BY PHASE-FIELD APPROACH

A Thesis in

Materials Science and Engineering

by

Chen Duan

Submitted in Partial Fulfillment
of the Requirements
for the Degree of

Master of Science

December 2012

The thesis of Chen Duan was reviewed and approved* by the following.

Long- Qing Chen
Professor of Materials of Science and Engineering
Thesis Adviser

Venkatraman Gopalan
Professor of Materials Science and Engineering

Roman Engel-Herbert
Assitant Professor of Materials Science and Engineering

Joan M. Redwing
Professor of Materials Science and Engineering
Chair, Intercollege Graduate Degree Program in Materials Science and Engineering

* Signatures are on file in the Graduate School

ABSTRACT

Ferroelectric materials are a class of important functional materials with wide applications in various fields, e.g., microelectronics, storage devices, sensors and actuators. The switching behaviors of ferroelectrics with applied electric field are fundamental to the storage applications. The traditional phenomenological thermodynamics is mainly based on perfect crystal model, which cannot properly describe the effect of ferroelectric domain wall as well as other defects. Besides, it cannot describe the switching with applied inhomogeneous electric field, which would be important to the nanoscale switching phenomena of with the tip of piezoresponse force microscopy (PFM).

Phase-field approach is a very powerful tool to model the microstructure evolution processes. In this work, a three-dimension phase-field model was developed to predict the nanoscale switching of ferroelectric thin film induced by the PFM tip. The nucleation mechanisms of reversal domain induced by the tip were intensively discussed which include the effects of a-c twinned domain wall and 180-degree domain wall. It is found that the effects are distance-dependent and the interaction between tip and a-c twinned domain wall is asymmetrical on the two sides. Besides, the mechanical effect induced by the PFM tip was also included, and the possibility of switching a single domain solely by mechanical means was confirmed, which may need further experimental confirmation.

TABLE OF CONTENTS

List of figures

List of Tables

Acknowledgement

I would like to express my sincere thanks to Dr Long-qing Chen for supervision, and his helpful guidance, great patience and encouragement during my two years' graduate study.

I also would like to thank Dr. V. Gopalan and Dr. Roman. Engel-Herbert for serving as my committee members of master defense and giving insightful comments. Besides, I am also grateful for our collaborators, Rama Vasudevan and Dr V. Nagaranjan in University of New South Wales, P. Gao, C. Nelson, Dr X.Q. Pan in University of Michigan and, Dr. S.V. Kalinin in Oak Ridge National Laboratory. For my current and previous labmates, Dr L. Y. Liang, Dr. L. Hong, Dr. T. W. Heo, Dr. B. Winchester, Dr. P. P. Wu, J. Briston, Y. Cao, Y. J. Gu, F. Xue, W. T. Xing, etc., special thanks are given to you for your comments in our discussions. I will also thanks for the financial supports from DOE, NSF, CCMD for my research.

Chapter 1 Research Background

1.1 Introduction

1.1.1 Ferroelectric Materials

Ferroelectric materials are certain classes of materials possessing spontaneous polarization without external electric field, which can be reoriented between crystallographically permitted states under sufficient external electric field [1]. The ferroelectricity can be traced back to Valasek's discovery on Rochelle salt [2]. Over almost a hundred years of development, ferroelectric materials are emerging as very crucial materials in engineering applications. The major technological aspects include: (1) Ultra-density Data storage [3] (e.g., FeRAM) which utilizes the polarization as binary data such that two opposite polarizations represent 0 or 1 data bits. Such ultra-density storage devices are predicted to have densities of 10 Tbit/in^2 and long retention times (~70 years). (2) Transducer [4]: Piezoelectric sensors that based on the conversion between mechanical energy and electrical energy through strong coupling between polarization and the structure of materials. (3) Capacitor applications led by generally large permittivity of ferroelectrics.

The most typical class of ferroelectrics are known as perovskite oxides, which have ABO_3 crystal structure as shown in Fig 1.1, where A and B represent cation elements, anion elements, respectively. The high-temperature paraelectric phase has a ***Pm3m*** cubic space group and in this case the A and B has only two equivalent configurations, e.g, if A occupies corner positions, the center positions will be occupied by B and the face center positions oxygen atoms, and vice versa. At paraelectric phase, the center of cations and anions are overlaid so as to

maintain macroscopically electro-neutral state. At paraelectric-ferroelectric transition temperature (known as Curie temeperature), the crystal structure of perovskite oxide will transform from cubic phase to a ferroelectric tetragonal phase (space group *P4mm*) such that a spontaneous polarization is generated with the displacement of cations and anions. The induced electric dipole is given by $\boldsymbol{p}=q\boldsymbol{r}$, where q is the charge and **r** is the relative displacement vector pointing from negative charge to positive one. The occurrence of spontaneous polarization is also accompanied by the distortion of lattice constants and thus led to a spontaneous strain given by $e_{ij}^{\ 0} = Q_{ijkl} P_k P_l$, where is Q_{ijkl} the electrostrictive coefficients.

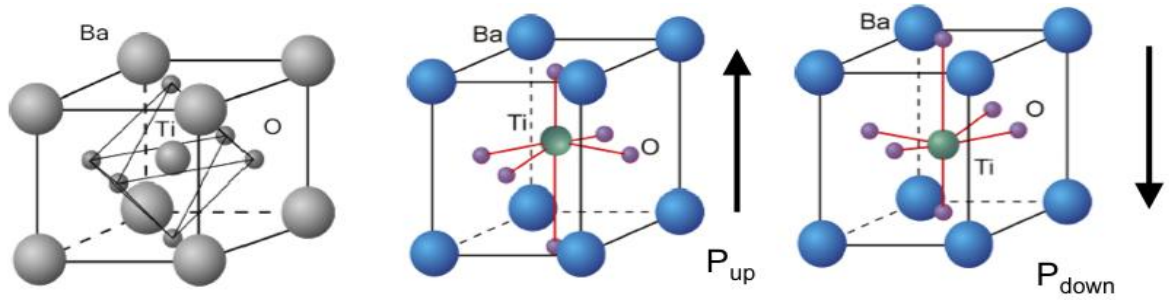

Fig 1.1 Schematic diagram of pervoskite structure (ABO_3) and the induced polarization associated with ionic displacement.

The spontaneous polarizations in real ferroelectric materials are generally not uniformly oriented along the same direction. However, in a certain region the spontaneous polarizations are uniformed oriented to minimize the dipole-dipole energy. These regions are known as ferroelectric domains, and the boundaries between different domains are known as domain walls. Many factors can affect the size and distribution of domains. For instance, there will be electrical energy accompanied by the generation of inhomogenous distribution of polarization. The mechanical boundary condition (applied strain and stress) can also greatly impact the domain structures [5], which is crucial in strain engineering of ferroelectric thin film. The equilibrium

domain structures are determined by minimizing the total free energy including bulk energy, elastic energy, electric energy and defect energy (for example, domain wall energy).

In rhombohedral ferroelectric materials (such as $BiFeO_3$), the polarization is along eight <111> crystal axes of paraelectric cubic unit cell, leading to 180 degree, 109 degree ad 71 degree domain walls. In tetragonal ferroelectrics (e.g., $PbTiO_3$), the polarization is along six <100> crystal axes of paraelectric cubic unit cell, and thus the possible domain walls are 180 degree and 90 degree. The 180 degree domain walls are pure ferroelectric while non-180 degree domain walls are both ferroelectric and ferroelastic since they differ from both spontaneous polarizations and spontaneous strains. The arrangement of polarization orientation between two neighboring domains are governed by electrostatic compatibility such that for 180 degree domain walls, the polarizations are anti-paralleled while for non-180 degree domain walls head-to-tails alignments are typical.

1.1.2 Thermodynamics of Polarization Switching

Generally, the thermodynamics of equilibrium system is described by a set of independent variables. For ferroelectric system, the set of independent variables are chosen from three classes of conjugate pairs: temperature T and entropy S, stress tensors s_{ij} and strain tensors e_{ij}, and electric field vectors E_i and polarization vectors P_i.

Following the first law and second law of thermodynamics, the change of internal energy can be given by

$$dU = TdS + s_{ij}de_{ij} + E_i dP_i \tag{1.1}$$

If using Helmholtz free energy $A(T, e_{ij}, P_i) = U - TS$ or elastic Gibbs free energy,

$G(T, s_{ij}, P_i) = U - TS - s_{ij}e_{ij}$ as state function, the equation can reduced into

$$dA = -SdT + s_{ij}de_{ij} + E_i dP_i \tag{1.2}$$

$$dG = -SdT + e_{ij}ds_{ij} + E_i dP_i \tag{1.3}$$

According to Landau-Devonshire phenomenological theory [6], for a centrisymmetric materials, the Gibbs potential can be described by a simple polynomial of polarizations, e.g.,

$$G = \frac{a}{2}P^2 + \frac{b}{2}P^4 + \frac{g}{2}P^6 \tag{1.4}$$

For simplicity, the b and g are set to be independent of temperature and a satisfies linear relation near the Curie temperature

$$a = a_0(T - T_c) \tag{1.5}$$

For a second-order paraelectric-ferroelectric transition, we can describe it by using fourth-order Gibbs potential

$$G = \frac{a_0(T - T_c)}{2}P^2 + \frac{b}{2}P^4 \tag{1.6}$$

According to Fig 1.2, above Curie temperature the Gibbs potential has only one minima at P=0 while, it will exhibit two stable states at + Ps and - Ps below curie temperature. That's how paraelectric-ferroelectric transition occurs.

The electrical field is given by

$$E = \frac{\partial G}{\partial P}\Big|_{T, s_{ij}} = a_0(T - T_c)P + b P_3 \tag{1.7}$$

which can describe the E-P Loop relationship as shown in Fig 1.2 (c)

The spontaneous polarization is deduced by the case without electrical field

$$P_S = \pm\sqrt{\frac{a_0}{b}(T - T_c)} \tag{1.8}$$

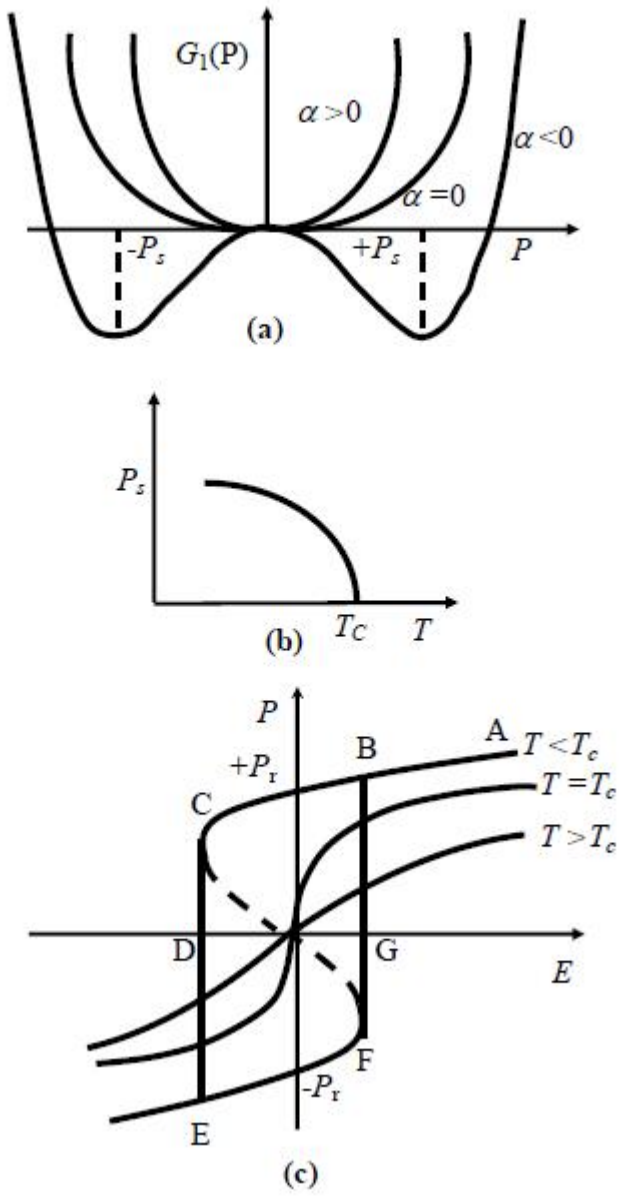

Fig 1.2 (a) Plot for Gibbs potential versus polarization for second-order paraelectric-ferroelectric transition near Curie temperature. (b) Plot for spontaneous polarization versus temperature (c) Plot for Polarization versus applied electric field

1.1.3 Piezoresponse Force Microscopy: Detection of Polarization Switching

Over recent decades, the scanning probe microscopy (SPM) has been extensively used as an instrumental means to probe local phase transition phenomena. The external stimulus is applied to the materials to induce phase transition, and the local changes of associated properties are detected by the SPM tip. A particular powerful case is Piezoresponse Force Microscopy (PFM). In PFM, external electric field is applied with the tip and through the coupling between electric field and mechanical strain which is important in ferroelectrics and other polar materials.

The principle of PFM is based on the interaction of applied electric field and polarization. The polarization will elongate with a paralleled electric field with an induced positive electromechanical deformation, and dwindle with an anti-paralleled electric field with a negative deformation. PFM experiments utilize a basic setup of atomic force microscopy with standard deflection-based feedback or contact mode imaging, in which an electrically conductive tip at then end of a cantilever is in contact with the piezoelectric sample (As shown in Fig.1.3). When a voltage is applied, the resulting deformation is measured based on variations of amplitude and phase of piezoresponse with AC bias. According to the direction of deformation, the PFM consists of vertical PFM and lateral PFM.

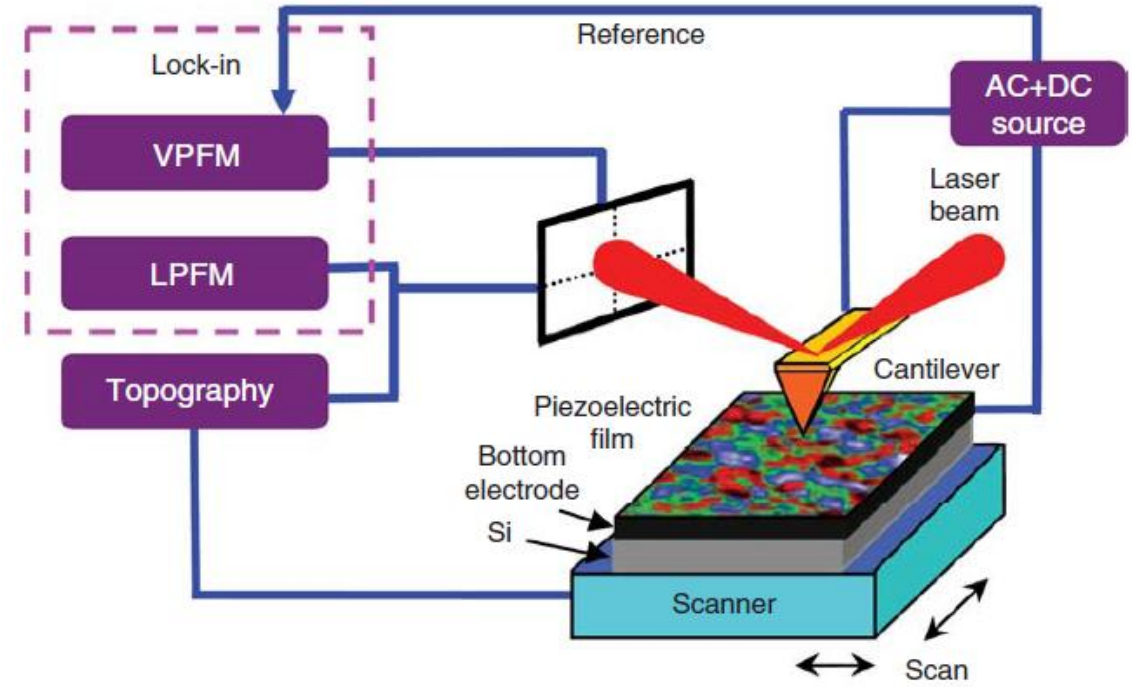

Fig. 1.3 Basic experimental setup of PFM measurement (Cited from [7]).

PFM was first demonstrated in 1992 to study ferroelectric polymer thin film [8]. In recent years, PFM has emerged as a powerful technique to study the local switching behavior in ferroelectric materials [9]. In PFM measurement, nucleation events are induced by local inhomogeneous field beneath the tip, offering a possibility of nanoscale probe of local switching behavior and microstructure as low as 10nm. To be specific, the domain structure can be visualized by monitoring the piezoresponse signal. The amplitude of this signal depends on the intensity of electromechanical, i.e., piezoelectric coefficient tensors. The phase of piezoresponse signal relies on the sign of piezoelectric coefficient (and therefore the direction of polarization) and, become reverse when the piezoelectric coefficient is opposite. In other words, the region of opposite region of polarization will counter with each other in phase contrast and vary with each other in amplitude. The two major approaches of the setup of PFM experiments are (1) A tip

generated inhomogeneous electric field and (2) A homogeneous field applied via top electrode contact of the sample. In both case, the tip serves as a local detection of electromechanical deformation induced by local (tip electrode) or uniform (top electrode) field. The rapid progress of PFM has evoked great advances in both theoretical models for imaging and control mechanism [10-12] and experimental observations in domain dynamics [13], ferroelectric lithography [14], and hyperfine structure of hysteresis loop [15], etc.

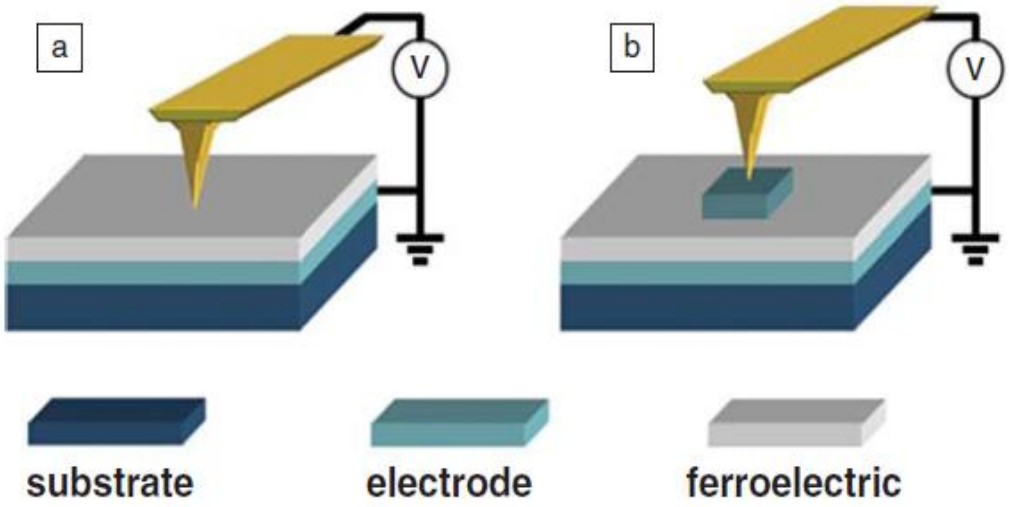

Fig1.4 Two geometry configurations of PFM measurement [7] (a) tip electrode (b) top electrode.

1.2 Research Objectives

As is discussed above, the domain stability and structures of ferroelectric thin film are decided by minimization of total free energy. Many aspects can affect the total free energy such as mechanical and electrical boundary condition, presence of free carrier and local defect, as well as the size and shape of thin film, involving long-range interactions like elastic interaction and electrostatic interaction, especially due to the inhomogeneous distribution of stress field and

electric field. This thesis will mainly study the interaction of domain wall and inhomogeneous field beneath a PFM tip. The specific objectives include:

(1) To investigate the effect of 180 degree ferroelectric domain wall on local switching

(2) To investigate the effect of ferroelastic a-c twinned domain wall on local switching

(3) To investigate the switching of ferroelastic domain by pure mechanical means

1.3 Thesis structure

Chapter 1 consists of general background of ferroelectricity and its detection by Piezoresponse Force Microscopy (PFM), followed by research objectives and thesis structure.

In Chapter 2, an introduction to phase field approach is given, and how it applied to model ferroelectric materials is discussed specifically.

In Chapter 3, the effect of 180 degree ferroelectric domain wall on local switching are studied, and various switching mechanism are discussed according to the distance between tip and domain wall.

In Chapter 4, the effect of ferroelasitic a-c twinned domain wall on local switching are studied, and the different switching mechanisms are found on the two sides of a domain.

In Chapter 5, we found ferroelectric thin film with a single domain can be possibly switched by inhomogeneous stress field applied by non-conductive AFM tip.

Chapter 6 concludes the thesis and some possible future works are discussed.

References

[1] M. Lines & A. Glass *Principles and applications of ferroelectrics and related materials*. Oxford (1979).

[2] J. Valasek, Phys. Rev. **17**, 475 (1921).

[3] P. Muralt, R. G. Polcawich, S. T-Mckinstry, MRS Bulletin. **34**, 658 (2009).

[4] T. M. Shaw, S. Mckinstry and P. C. McIntyre, Annu. Rev. Mater. Res. **30**, 263(2000).

[5] D. G. Scholm, L.Q. Chen, C. B. Eom, K. M. Rabe, S.K. Streiffer, J. M. Triscone, Annu. Rev. Mater. Res. **37**, 589(2007).

[6] A.F. Devonshire, Adv. Phys. **3**, 85 (1954).

[7] S. V. Kalinin, N. Setter, A. L. Kholkin, MRS Bulletin. **34**, 634 (2009).

[8] P. Guthner and K. Dransfeld, Appl. Phys. Lett. **61**, 1337(1992).

[9] S. V. Kalinin, A. N. Morozovska, L. Q. Chen and Brian J Rodriguez, Rep. Prog. Phys. **73**, 056502(2010).

[10] E. A. Eliseev, S. V. Kalinin, S. Jesse, S. L. Bravina, and A. N. Morozovska, J. Appl. Phys. **102**, 014109 (2007).

[11] A. N. Morozovska, E. A. Eliseev, and S.V. Kalinin, J. Appl. Phys. **102**, 074105 (2007).

[12] S.V. Kalinin, E. A. Eliseev, and A. N. Morozovska, Appl. Phys. Lett. **88**, 232904 (2006).

[13] C.T. Nelson, et.al., Science **334**, 96 (2011).

[14] Ji Young Jo et.al. Nano Lett. **11**, 3080 (2011).

[15] A. Kumar, O. S. Ovchinnikov, H. Funakubo, S. Jesse, and S. V. Kalinin Appl. Phys. Lett. **98**, 202903 (2011).

Chapter 2 Methodology

2.1 Phase Field Approach

Phase field approach is a very powerful technique widely applied to investigate the microstructure evolution of a great deal of materials at mesoscale [1]. In this approach, the microstructure information of both composition and domains are defined by a certain sets of field variables. Such field variables vary continuously across the domains or interfaces, so that the interfaces are described diffusedly instead of conventional sharp-interface model. There are two types of field variables: conversed and non-conversed. The conversed field variables must satisfy local conservation conditions, e.g. continuous equations, while non-conversed ones don't. The typical field variables include compositions of equilibrium system, long-range structural order parameter in phase transition process, polarization in ferroelectric materials, and magnetization in ferromagnetic materials, etc. In phase–field modeling, the thermodynamics and kinetics parameters are employed as inputs and an initial microstructure are given. The evolution process and final equilibrium microstructure are obtained by calculation of the driving forces. Depending on the type of field variables, the governing evolution equations are Cahn-Hilliard non-linear diffusion equations for conversed field variables [2] and Allen-Cahn equations (time-dependent Landau-Ginzburg equations) [3] for non-conversed field variables:

Cahn-Hilliard Equations $$\frac{\partial c_i(r,t)}{\partial t} = \nabla M_{ij} \nabla \frac{dF}{dc_j(r,t)} \tag{2.1}$$

Allen-Cahn Equations $$\frac{\partial h_q(r,t)}{\partial t} = -L_{pq} \frac{dF}{dh_q(r,t)} \tag{2.2}$$

where L_{pq} and M_{ij} are the kinetics parameters related to atomic or interface mobility, c_i and h_q are conversed field variables and non-conversed field variables, respectively. Modeling of the microstructure is reduced to solving the above equations by numerical methods. A number of numerical methods can be implemented. The simplest method is second-order finite-difference approach using uniform grid spacing and explicit time-stepping. However, the stability of this technique requires a very small time step, which increases a tremendous of computational resource. With periodic boundary condition, one of the cost-effective methods is spectral metod with Fast Fourier Transform. Recently, a very efficient semi-implicit fourier spectral method has been applied to solve the phase-field equations [4]. Since there is no interface-tracking, the phase field approach can be easily employed to study complicated 3D microstructures without a prior assumption. In past decades, the applications of phase field approach are increasingly expanding, from spinodal decomposition [5], martensite phase transformation [6], solidification [7], grain growth [8], to complex domain structure in ferroelectric materials [9], multiferroics [10], as well as electrochemical applications [11].

2.2 Phase Field Modeling of Ferroelectrics

In ferroelectrics, the main field variables are polarizations, which is non-conserved. Therefore, the evolution of 3D polarization field is governed by Allen-Cahn type of equations.

$$\frac{\partial P_i(\mathbf{x},t)}{\partial t} = -L\frac{dF}{dP_i(\mathbf{x},t)}, i = 1,2,3 \tag{2.3}$$

where L is a kinetic coefficient related to the domain wall mobility. F is the total free energy of the system, which can be calculated by

$$F = \int (f_{bulk} + f_{grad} + f_{elas} + f_{elec})dV \tag{2.4}$$

The mathematical expression of ferroelectric bulk free energy density f_{bulk}, e.g., Landau potential is given by Devonshire [12]

$$f_{bulk} = \frac{1}{2}a_{ij}P_iP_j + \frac{1}{3}b_{ijk}P_iP_jP_k + \frac{1}{4}g_{ijkl}P_iP_jP_kP_l + \frac{1}{5}d_{ijklm}P_iP_jP_kP_lP_m + \frac{1}{6}w_{ijklmn}P_iP_jP_kP_lP_mP_n + \ldots \tag{2.5}$$

If the material is centresymmetric, all the odd terms will be absent, the expression is reduced to

$$f_{bulk} = \frac{1}{2}a_{ij}P_iP_j + \frac{1}{4}g_{ijkl}P_iP_jP_kP_l + \frac{1}{6}w_{ijklmn}P_iP_jP_kP_lP_mP_n + \ldots \tag{2.6}$$

For typical materials, we can employ fourth-order expression to describe second-order ferro-para transition while six-order or eight-order for first-order transition. The general expression is,

respectively,

$$f_{bulk} = a_1(P_1^2 + P_2^2 + P_3^2) + a_{11}(P_1^4 + P_2^4 + P_3^4) + a_{12}(P_1^2P_2^2 + P_2^2P_3^2 + P_1^2P_3^2)$$

(2.7)

$$f_{bulk} = a_1(P_1^2 + P_2^2 + P_3^2) + a_{11}(P_1^4 + P_2^4 + P_3^4) + a_{12}(P_1^2P_2^2 + P_2^2P_3^2 + P_1^2P_3^2)$$
$$+a_{111}(P_1^6 + P_2^6 + P_3^6) + a_{112}[P_1^4(P_2^2 + P_3^2) + P_2^4(P_1^2 + P_3^2) + P_3^4(P_1^2 + P_2^2)] + a_{123}P_1^2P_2^2P_3^2$$

(2.8)

$$f_{bulk} = a_1(P_1^2 + P_2^2 + P_3^2) + a_{11}(P_1^4 + P_2^4 + P_3^4) + a_{12}(P_1^2P_2^2 + P_2^2P_3^2 + P_1^2P_3^2)$$
$$+a_{111}(P_1^6 + P_2^6 + P_3^6) + a_{112}[P_1^4(P_2^2 + P_3^2) + P_2^4(P_1^2 + P_3^2) + P_3^4(P_1^2 + P_2^2)] + a_{123}P_1^2P_2^2P_3^2$$
$$+a_{1111}(P_1^8 + P_2^8 + P_3^8) + a_{1112}[P_1^6(P_2^2 + P_3^2) + P_2^6(P_1^2 + P_3^2) + P_3^6(P_1^2 + P_2^2)]$$
$$+a_{1122}(P_1^4P_2^4 + P_2^4P_3^4 + P_1^2P_3^2) + a_{1123}(P_1^4P_2^2P_3^2 + P_2^4P_1^2P_3^2 + P_3^4P_1^2P_2^2)$$

(2.9)

Typically, the expansion of first term a_1 is linear proportional to temperature, e.g, $a_1 = a_1(T - T_0)$ where T_0 is the Curie transition temperature of ferroelectric-paraelectric transition. For specific materials, the expression of this energy is also subject to crystal symmetry and some of the expansion coefficient will be absent accordingly.

The gradient energy density f_{grad} is given by

$$f_{grad} = \frac{1}{2}G_{ijkl}P_{i,j}P_{k,l}$$

(2.10)

where $P_{i,j} = \partial P_i / \partial x_j$, G_{ijkl} is the gradient energy coefficients. In general, the gradient energy is anisotropic. However, we assume cubic symmetry for the sake of simplicity. The expression can be therefore expressed as

$$\begin{aligned} f_{grad} &= \frac{1}{2}G_{11}(P_{1,1}^2 + P_{2,2}^2 + P_{3,3}^2) + G_{12}(P_{1,1}P_{2,2} + P_{2,2}P_{3,3} + P_{1,1}P_{3,3}) \\ &+ \frac{1}{2}G_{44}[(P_{1,2} + P_{2,1})^2 + (P_{2,3} + P_{3,2})^2 + (P_{1,3} + P_{3,1})^2] \\ &+ \frac{1}{2}G_{44}'[(P_{1,2} - P_{2,1})^2 + (P_{2,3} - P_{3,2})^2 + (P_{1,3} - P_{3,1})^2] \end{aligned} \tag{2.11}$$

The elastic energy density f_{elas} is given by

$$f_{elas} = \frac{1}{2}c_{ijkl}(e_{ij} - e_{ij}^{\,0})(e_{kl} - e_{kl}^{\,0}) \tag{2.12}$$

where e_{ij} and $e_{ij}^{\,0}$ is the total strain and eigenstrain, c_{ijkl} is the elastic constants. Under stress-free boundary condition, the eigenstrain be can expressed as [12]

$$\begin{aligned} e_{11}^{\,0} &= Q_{11}P_1^2 + Q_{12}(P_2^2 + P_3^2) \\ e_{22}^{\,0} &= Q_{11}P_2^2 + Q_{12}(P_1^2 + P_3^2) \\ e_{33}^{\,0} &= Q_{11}P_3^2 + Q_{12}(P_1^2 + P_2^2) \\ e_{23}^{\,0} &= Q_{44}P_2\,P_3 \\ e_{13}^{\,0} &= Q_{44}P_1\,P_3 \\ e_{12}^{\,0} &= Q_{44}P_1\,P_2 \end{aligned} \tag{2.13}$$

where are Q_{11}, Q_{12}, Q_{44} electrostrictive coefficients based on cubic assumption.

The electrostatic energy density of a polarization vector field is given

$$f_{elec} = -\frac{1}{2} e_0 k_{ij} E_i E_j - E_i P_i \tag{2.14}$$

where Ei is the i th component of the electric field and e_0 is the dielectric permittivity of the vacuum and k_{ij} is the background dielectric constant of the ferroelectric film [13]. The specific deviation is shown as follows, with perfect screening condition on the surface ($r_f = 0$)

$$\begin{aligned}
F_{elec} &= \int_V d^3 r \frac{\vec{D} \bullet \vec{E}}{2} + \int_S d^3 r j\, D_n \\
&= \int_V d^3 r [\frac{\vec{D} \bullet \vec{E}}{2} + \nabla \bullet (j\, \vec{D})] \\
&= \int_V d^3 r (\frac{\vec{D} \bullet \vec{E}}{2} + j \nabla \bullet \vec{D} + \vec{D} \nabla j\ ) \\
&= \int_V d^3 r (-\frac{\vec{D} \bullet \vec{E}}{2} + j\, r_f\ ) (with \nabla \bullet \vec{D} = r_f, \nabla j\ = -\vec{E}) \\
&= \int_V d^3 r (\frac{a_{ij}}{2} P_i P_j - \frac{1}{2} e_0 k_{ij} E_i E_j - E_i P_i) (with D_i = P_i + e_0 k_{ij} E_j, \vec{E} = a\, \vec{P}, r_f = 0)
\end{aligned}$$

The first term is the contribution of soft mode of polarization and can be integrated into the second order term of the Landau potential. Therefore, the electrostatic energy density associated with external field is approximately given by $f_{elec} = -\frac{1}{2} e_0 k_{ij} E_i E_j - E_i P_i$.

Besides solving Allen-Chan equations to obtain temporal evolution process, the system must also satisfy simultaneously both elastic and electrostatic equilibrium with a certain elastic and electrical boundary condition.

With respect to mechanical equilibrium, following the Khachaturyan theory [14], the total strain can be decomposed into homogenous strain $\overline{e_{ij}}$ and heterogeneous strain de_{ij}

$$e_{ij} = \overline{e_{ij}} + de_{ij} \tag{2.15}$$

The homogenous part characterizes the macroscopic shape change. For a coherent thin film, the homogenous strain is totally controlled by the substrate misfit. For example, for cubic substrate, the misfit strain is given by,

$$\overline{e_{11}} = \overline{e_{22}} = \frac{a_s - a_f}{a_s}, \overline{e_{33}} = 0 \tag{2.16}$$

where a_s and a_f is the lattice constant of substrate and thin film, respectively. The heterogeneous part satisfies

$$\int_V de_{ij} d^3 r = 0 \tag{2.17}$$

which can be also expressed by the partial derivative of mechanical displacement.

$$de_{ij} = \frac{1}{2}\left(\frac{\partial u_i}{\partial x_j} + \frac{\partial u_i}{\partial x_j}\right) \tag{2.18}$$

The mechanical equilibrium equation and Hooke's Law are

$$\frac{\partial s_{ij}}{\partial x_j} = 0 \tag{2.19}$$

$$s_{ij} = c_{ijkl}(e_{ij} - e_{ij}^{\,0}) \tag{2.20}$$

For a thin film system with a substrate in Fig.2.1, the stress-free boundary condition is

$$s_{i3}\big|_{x=h_f} = 0 \tag{2.21}$$

where h_f is the thickness of thin film. With displacement as variable, the mechanical equilibrium equation and boundary condition can be reduced to

$$c_{ijkl}\frac{\partial^2 u_k}{\partial x_l \partial x_j} = c_{ijkl}\frac{\partial e_{ki}^{\ 0}}{\partial x_j} \tag{2.22}$$

$$c_{ijkl}\left(\frac{\partial u_k}{\partial x_l} - e_{kl}^{\ 0}\right)\Big|_{x_3 = h_f} = 0 \tag{2.23}$$

The clamping condition of substrate (h_s is the distance into substrate that deformation effect is absent.)

$$u_i\,|_{x_3 = -h_s} = 0 \tag{2.24}$$

The solution of such mechanical equilibrium equation with mixed thin film boundary condition can be divided into two steps. The first step is to solve the mechanical equilibrium equation with Khachaturyan theory in 3D space with eigenstrain distribution within $0 < x < h_f$. The second step is to find the elastic solution of an infinite plate of thickness $h_f + h_s$, but with modified boundary condition according to the first part of solution. The final solution is the superposition of these two parts. Specific solution techniques can be found in Ref 17.

For ferroelectric system, the electrostatic equilibrium equation can be expressed as Poisson type with $D_i = P_i + e_0 k_{ij} E_j$ and $E_j = -\frac{\partial j}{\partial x_j}$,

$$e_0 k_{ij}\frac{\partial^2 j}{\partial x_i \partial x_j} = \frac{\partial P_i}{\partial x_i} \tag{2.25}$$

With the assumption of isotropic dielectric constants, it can be reduced to

$$e_0\left(k_{11}\frac{\partial^2 j}{\partial x_1^2} + k_{22}\frac{\partial^2 j}{\partial x_2^2} + k_{33}\frac{\partial^2 j}{\partial x_3^2}\right) = \frac{\partial P_1}{\partial x_1} + \frac{\partial P_2}{\partial x_2} + \frac{\partial P_3}{\partial x_3} \tag{2.26}$$

The electrical boundary conditions for a thin film system include two types: open-circuit or

closed-circuit. For the open-circuit boundary condition, the electric displacement on the top and bottom surface is equal to zero (Neumann type boundary condition), with surface charge left

$$e_0 k_{ij} \frac{\partial j}{\partial x_j} |_{surface} = P_i \tag{2.27}$$

For the closed-circuit one, the potentials on the top and bottom surface are given (Dirichlet boundary condition).

$$j_{bottom} = j_1, j_{top} = j_2 \tag{2.28}$$

Specifically, the short-circuit boundary condition indicate the case of $j_1 = j_2$. The solution technique of this equation with boundary condition is very similar to that of mechanical equilibrium equation by superposition method.

For the electrode configuration here, the electrostatic equilibrium equation is solved using a specified boundary condition on the bottom and top of the thin film, with prefect screening of surface charge.

$$j_{bottom} = 0, j_{top} = j(x, y) \tag{2.29}$$

To simulate the effect of PFM probe, the tip potential on the top surface of thin film is approximately implemented by a Lorentz distribution

$$j(x, y) = j_0 \frac{g^2}{g^2 + (x - x_0)^2 + (y - y_0)^2} \tag{2.30}$$

where j_0 is the center value of tip potential and (x0, y0) are tip coordinates, and γ is the half-width of the tip.

The numerical solution of phase field evolution of ferroelectrics requires normalization of physical quantities. In the equations, the polarizations are normalized by the spontaneous polarization and the time is normalized by kinetic coefficient and first-order expansion coefficient of landau free energy. The other physical quantities are normalized too.

$$
\begin{aligned}
&P^* = P / P_0 \\
&t^* = t / t_0, t_0 = (a_0 L)^{-1} \\
&r^* = r / l_0, l_0 = \sqrt{G_{11} / a_0} \\
&F^* = F / (a_0 P_0^2) \\
&E^* = E / (a_0 P) \\
&j^* = j / (a_0 P_0 l_0) \\
&s^* = s / (a_0 P_0^2) \\
&u^* = u / l_0
\end{aligned}
\tag{2.31}
$$

Thus, the normalized phase field evolution equation is reduced to

$$
\frac{\partial P_i^*(\mathbf{x},t)}{\partial t^*} = -\frac{d F^*}{d P_i^*(\mathbf{x},t)} \tag{2.32}
$$

Using fourier transform, the evolution equation in k-space is

$$
\frac{\partial \overline{P_i^*}(\mathbf{x},t)}{\partial t^*} = -\frac{d F^*}{d P_i^*(\mathbf{x},t)} \tag{2.33}
$$

With semi-implicit scheme, the evolution of polarizations in k-space are governed by

$$
\overline{P_i^*}^{n+1}(\mathbf{r}k,t) = \frac{\overline{P_i^*}^{n}(\mathbf{r}k,t) + \Delta t\, \overline{f_i^*}(\mathbf{r}k,t)}{1 + \Delta t k_{Gi}^2}
$$

$$\overline{f_i^*}^{\mathbf{r}}(k,t) = F\{-\frac{\partial}{\partial P_i}(f_{bulk}^* + f_{elas}^* + f_{elec}^*)\}$$

$$k_{G1}^2 = G_{11}k_1^2 + (G_{44} + G_{44}^{'})(k_2^2 + k_3^2)$$

$$k_{G2}^2 = G_{11}k_2^2 + (G_{44} + G_{44}^{'})(k_1^2 + k_3^2)$$

$$k_{G3}^2 = G_{11}k_3^2 + (G_{44} + G_{44}^{'})(k_1^2 + k_2^2)$$

(2.34)

The real-space polarizations can be then obtained by doing inverse Fourier transform.

References

[1] L. Q. Chen, Ann. Rev. Mater. Res. **32**, 113 (1998).

[2] J. W. Cahn, Acta. Metalla. **9**, 795 (1961).

[3] S. M. Allen and J. W. Cahn, J. de Phys. **38**, C7 (1977).

[4] L. Q. Chen and J. Shen, Comput. Phys. Commun. **108**, 147 (1998).

[5] H. Nishimori and A. Onuki. Phys. Rev. B **42**, 980 (1990).

[6] Y. M. Jin, A. Artemev, A.G. Khachaturyan Acta Mater.**49**, 2309 (2001).

[7] J. S. Langer, *Directions in Condensed Matter Physics*. Philadelphia (1986).

[8] C. E. Krill and L. Q. Chen, Acta Mater. **50**, 3057 (2002).

[9] Y. L. Li, S. Y. Hu, Z.K. Liu and L. Q. Chen, Appl. Phys. Lett. **78**, 3878 (2001).

[10] J. X. Zhang, Y. L. Li, Y. Wang, Z. K. Liu and L. Q. Chen, J. Appl. Phys. **101**, 114105 (2007).

[11] N. Balke, et.al., Nat. Nano. **5**, 749 (2010).

[12] A.F. Devonshire, Adv. Phys. **3**, 85 (1954).

[13] A. K. Tagantsev, Ferroelectrics **69**, 321 (1986).

[14] A.G. Khachaturyan, *Theory of Structural Transformation in Solids*. New York (1983).

[15] Y. L. Li, S. Y. Hu, Z. K. Liu, and L. Q. Chen, Acta Mater. **50**, 395 (2002).

Chapter 3 Effect of 180 Degree Domain Wall and 90 Degree Domain Wall on Local Switching of PZT Thin Film

3.1 Introduction

As one of the most common ferroelectrics, epitaxial $Pb_xTi_{1-x}O3$ (PZT) thin film has wide commercial applications in ultrasonic transducers and ferroelectric random access memory [1]. In the past decade, the local switching behavior of PZT thin film is mainly observed indirectly by PFM [2-5] based on the piezoresponse under bias applied by the tip while the atomic scale observation of domain structure of PZT thin film by TEM has been traced back to Jia [6]. Recently, Gao and Nelson [7] employed in situ TEM to observe directly the retention behavior of localized 180 degree switching in PZT thin film. Later, they [8] also studied the role of defect and confirmed the effects of interface and dislocations.

With regard to theoretical models of local polarization switching, the pioneering work of Landuaer [9] on ferroelectric domain nucleation with uniformed electric field showed that the discrete switching centers contribute more to nucleation events under a low electric field. At nanoscale level, the model for the nucleation mechanism under inhomogeneous field of local tip has been proposed by Molotskii [10] in 2004. Further theories on domain switching mechanisms in PFM were presented by Morozovska for a single domain as well as that with 180- degree ferroelectric wall [11, 12]. Although previous phase-field simulations has been presented for single domain [13, 14], single ferroelectric wall [15] and ferroelastic wall [16], the details of polarization switching was only theorized by analytical 1D model.

In this chapter, a 3D phase-field model will be developed to simulate the local switching phenomena of tetragonal ferroelectric thin film materials (PZT as an example). A uniform description to visualize the switching process is applied to single domain nucleation, and then to investigate the effect of typical domain wall in PZT thin film (180 degree ferroelectric wall, and 90 degree ferroelastic wall).

3.2 Domain Structure of PZT thin film

The phase diagram of PZT thin film has been measured many years ago by experiment and investigated by thermodynamics calculation [1]. Recently, it was recalculated by phase – field approach [17] and first-principle simulation[18]. These studies show almost consistent result in room temperature. In Zr-rich region, the phase is distorted rhombohedral, while the phase is tetragonal in Ti-rich, region, which is the major usable composition of PZT as tetragonal ferroelectrics. In the boundary region, i.e. morphotropic phase boundary (MPB), the PZT thin film is found to be mixed or monoclinic phase, which is promising for high dielectrics and enhanced electromechanical response, both experimentally[19] and theoretically[20].

For a typical tetragonal PZT thin film (e.g., PbTiO3), there are six variants for different domains, i.e., c^+ ($P_3>0$, $P_1=P_2=0$), c^- ($P_3<0$, $P_1=P_2=0$), a_1^+ ($P_1>0$, $P_2=P_3=0$), a_1^- ($P_1<0$, $P_2=P_3=0$), a_2^+ ($P_2>0$, $P_1=P_3=0$), a_2^- ($P_2<0$, $P_1=P_3=0$). The domain structure is shown to be controlled by substrate strain in a certain temperature. For example, the temperature-strain phase diagram of $PbTiO_3$ is shown in Fig 4.2. The domain structure of PbTiO3 at room temperature is shown in Fig 4.3. It is indicated that the c-domain are preferred on the compressive substrate strain and a domain on the tensile compressive substrate strain.

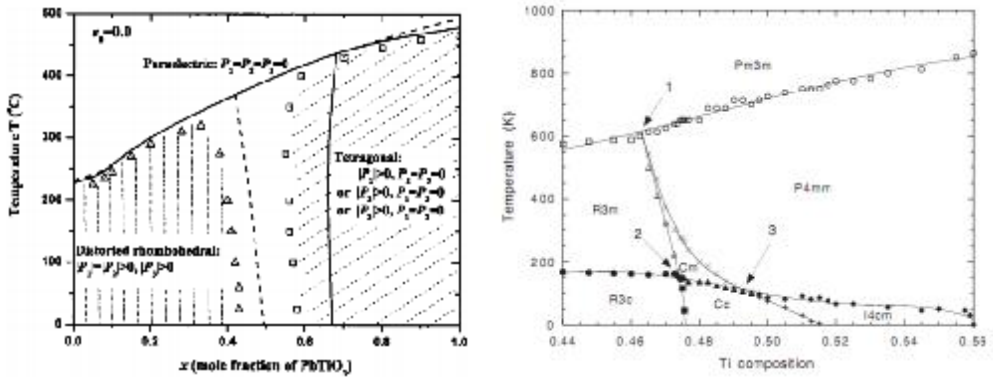

(a) (b)

Fig 3.1 (a) PZT phase diagram under stress-free condition calculated by thermodynamic model (solid line) and phase-field approach (scattered symbols) (b) PZT phase diagram near MPB calculated by first principle. The five phases in the diagram are Pm3m, cubic paraelectric phase, P4mm, tetragonal phase, R3m and R3c rhombohedral phase, cm as monoclinic phase.

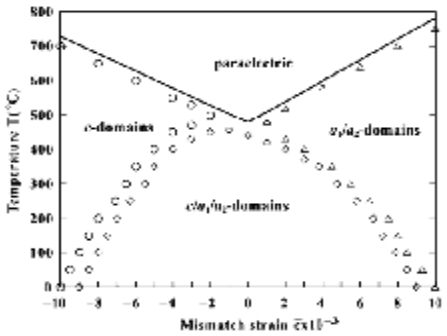

Fig 3.2 Temperature-strain phase diagram of PbTiO3 (solid line is the result of thermodynamics calculation and the scattered symbols are results calculated by phase-field approach)

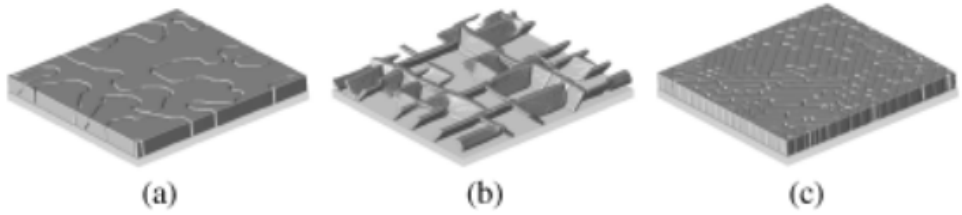

Fig 3.3 Domain structures of PbTiO3 at room temperature calculated by phase-field approach. (a) c-domain with 180 degree domain wall (ε = -1.2%) (a) c/a1/a2 domain structure (ε = -0.1%) (c) a1/a2 domain structure (ε = 1.2%)

3.3 Calculation Details

We found in the temperature-composition phase diagram of $Pi_xZr_{1-x}O_3$ is shown in Fig.4.1 (a) for a Ti-rich composition, the phase transition occurs with a crystallographically cubic to tetragonal transition. The six-order Landau potential we used is given by Haun [1].

$$f_{bulk} = a_1(P_1^2 + P_2^2 + P_3^2) + a_{11}(P_1^4 + P_2^4 + P_3^4) + a_{12}(P_1^2P_2^2 + P_2^2P_3^2 + P_1^2P_3^2)$$
$$+a_{111}(P_1^6 + P_2^6 + P_3^6) + a_{112}[P_1^4(P_2^2 + P_3^2) + P_2^4(P_1^2 + P_3^2) + P_3^4(P_1^2 + P_2^2)] + a_{123}P_1^2P_2^2P_3^2 \quad (3.1)$$

In our simulation, PZT (44/56) thin film is chosen as an example for tetragonal ferroelectric thin film Its expansion coefficients and materials constants can be calculated by the formula given by Haun [21] The elastic compliance constant for x= 0.4, 0.5, 0.6, 0.7, 0.8 0.9, which is given in the Table 4.1. We can obtain the elastic compliance constant of PZT (44/56) by spline interpolation technique. The materials constant at 300K for PZT (44/56) are given in Table 4.2.

Table 3.1 Elastic compliance constant for various Ti composition of PZT thin film [20]

Ti content x	0.4	0.5	0.6	0.7	0.8	0.9
s_{11} ($10^{-12}m^2/N$)	8.8	10.5	8.6	8.4	8.2	8.1
s_{12} ($10^{-12}m^2/N$)	-2.9	-3.7	-2.8	-2.7	-2.6	-2.5
S_{44} ($10^{-12}m^2/N$)	24.6	28.7	21.2	17.5	14.4	12.0

Table 3.2 Landau expansion coefficients of PZT (44/56) at 300K.

Landau coefficients	a_1 ($10^9C^{-2}m^{10}N$)	a_{11} ($10^9C^{-4}m^6N$)	a_{12} ($10^9C^{-4}m^6N$)	a_{111} ($10^9C^{-4}m^6N$)	a_{112} ($10^9C^{-6}m^{10}N$)	a_{123} ($10^9C^{-6}m^{10}N$)
Values	-6.45	4.05	0.24	0.16	0.71	-0.34

Table 3.3 Materials constants of PZT (44/56) at 300K.

Materials constants	s_{11} ($10^{-12}m^2/N$)	s_{12} ($10^{11}m^2/N$)	s_{44} ($10^{11}m^2/N$)	Q_{11} ($C^{-2}m^4$)	Q_{12} ($C^{-2}m^4$)	Q_{12} ($C^{-2}m^4$)
Values	9.1	-3.1	23.6	0.043	-0.017	0.036

The time-dependent Ginzburg-Landau equations are solved by semi-implicit Fourier method [22].We used a grid 128 Δx × 128 Δx × 36 Δx with periodic boundary conditions along x1 and x2 axes in the film plane. The spacing of grid Δx is set as 1nm. The thickness of film is taken as 20 Δx and 12 Δx for the effective thickness of the substrate layer. The substrate strains for ferroelectric and ferroelastic case are chosen as compressive 1% and 0.5% for elastic energy, respectively. The temperature used in our simulation is 300K.

To schematically show the interaction between tip and domain wall, we introduce another quantity called "wall twist", based on the variation of in-plane polarization, defined as

$$w = \int (P_{IP,f} - P_{IP,0V})^2 dV \tag{3.2}$$

where PIP is the magnitude of the in-plane polarization i.e. $(Px^2 + Py^2)^{1/2}$. The wall twist is thus a measure of the variation of the polarization as a result of applying voltage through the tip. Note the integration is performed over a small local region (volume), which is approximated as Δx_3 with our phase-field modeling

3.4 Results and Discussions

Firstly, we simply examine the intrinsic polarization reversal mechanism without presence of any defect in a single c- domain. For the sake of symmetry, the tip was placed in the center and the nucleation bias was calculated as 5.2V. The calculated hysteresis loop for local displacement is shown in Fig.1 (a), and the corresponding polarization distributions in A, B, C, D, E, F are also

shown in Fig.1.(b). Similar butterfly-like hysteresis loop was also observed by experiment for intrinsic switching of $BiFeO_3$ thin film [13].

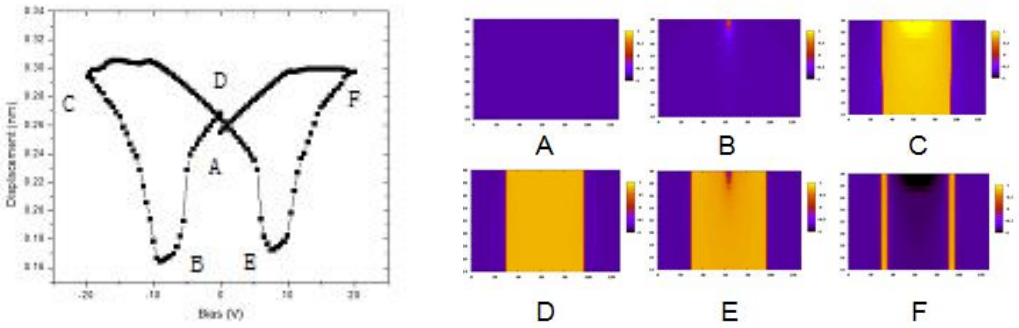

(a) (b)

Fig 3.4 (a) Local displacement loops. (b) Temporal evolution of out-of-plane polarization distribution in the thin film corresponding to A to F, cutting from x_2- x_3 plane.

To examine the switching process shown in Fig.1.in details, we start from a single c- domain as indicated by Point A. Nucleation of a reversal domain occurs when an anti-paralleled bias exceeds the nucleation bias (the Point B), where a needle-like geometry is achieved to reduce the area of 'head to head' charged domain wall. The newly-nucleated reversal domain will first penetrate into the film and then grow laterally after reaching the film/substrate interface. The main driving force in this stage is the vertical electric field at first, and then become lateral electric field due to the pinning effect of the substrate when the reversal domain reaches the substrate. Besides, the mechanism of backward nucleation is shown to be the case that the c- domain is nucleated within the matrix of nucleated reversal c+ domain instead of the dwindling of reversal domain, confirmed by the recent in situ TEM experiment [23].

To further investigate the effect of single ferroelectric wall, we consider a half c+ half c- stripe structure with a 180 degree domain wall of a width of 1nm as Fig.2 (a), close to the experimental results [17]. The tip was placed at various locations on the left side of domain wall

along the a-b-c as presented in Fig.2 (a). We add an anti- paralleled electric field to induce nucleation of reverse c+ domain. The nucleated bias profile is calculated as shown in Fig.2 (b). The trend is qualitatively consistent with phenomenological model [12]. At large separation between tip and domain wall (Fig.2.(c)), the nucleation process is almost the same as that of single domain. With the intermediate tip and domain wall distance (4nm from domain wall, shown in Fig.2(d)), the growth of domain on the near side of domain-wall is inhibited from needle-like, and the nucleation bias is increased due to effect of induced extra depolarization field associated with the ferroelectric wall. We can see that the values of bias in first two case is ranging from 5.2V to 6V similar to single domain nucleation (5.4V), reflecting that the range of the effect of ferroelectric is short (which contrasts with that of ferroelastic wall, which will be discussed in later section).If the tip placed on the domain wall (Fig.2.(e)), the nucleation is mainly due to the bending of nearby c+ domain, leading to very low nucleation bias. Our results can be similar to the experiment by Aravind et.al for $LiNbO_3$[15].

The nucleation mechanism with presence of ferroelectric wall can be categorized into three cases by Morozoska et.al.[14] (i) bulk nucleation, (ii) correlated nucleation and (iii) domain wall reversible bending. The corresponding nucleation and growth process are shown below. At large tip-wall separation, the mechanism will be bulk nucleation and growth, with tiny long-range effect (Fig.2(c)). The correlated nucleation will occur in the intermediate distance (Fig.2 (d)).When tip placed very close or at the wall, the domain bending mechanism will dominate (Fig.2 (e)). To further visualize the interaction between tip and domain wall, we perform calculation of wall twist for each cases, as shown on the right of Fig.2. (c), (d), (e). We can easily see that the wall twist of ferroelectric wall region in the case of (a) bulk nucleation is almost

invisible, and become important for correlated mechanism, and then (c) the major driving force of nucleation for domain bending mechanism.

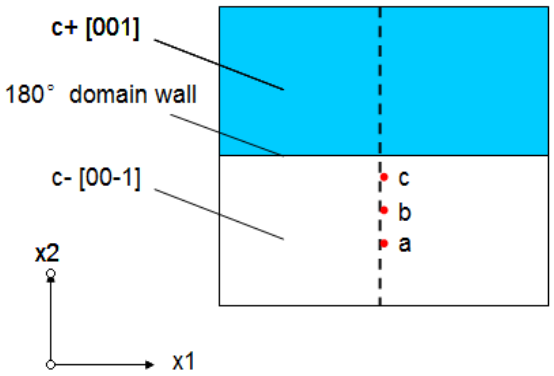

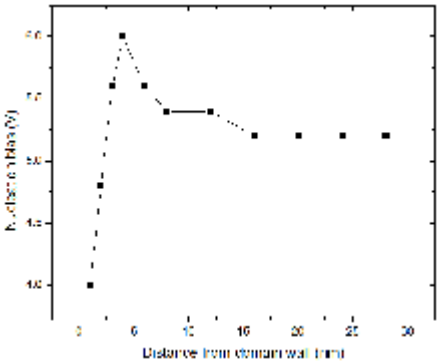

(a) **(b)**

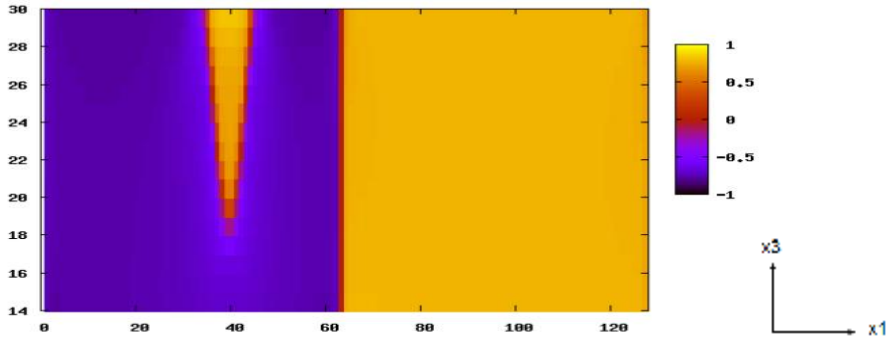

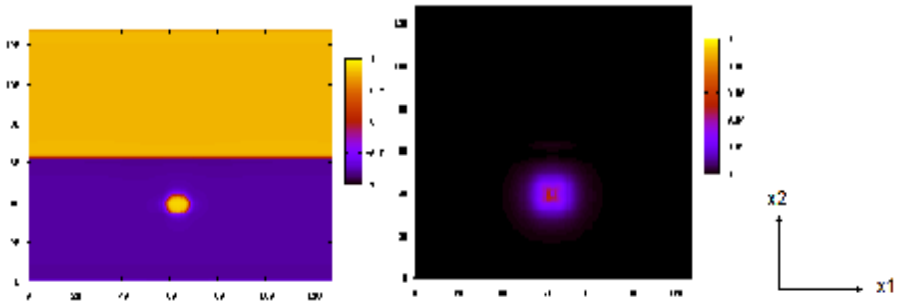

(c)

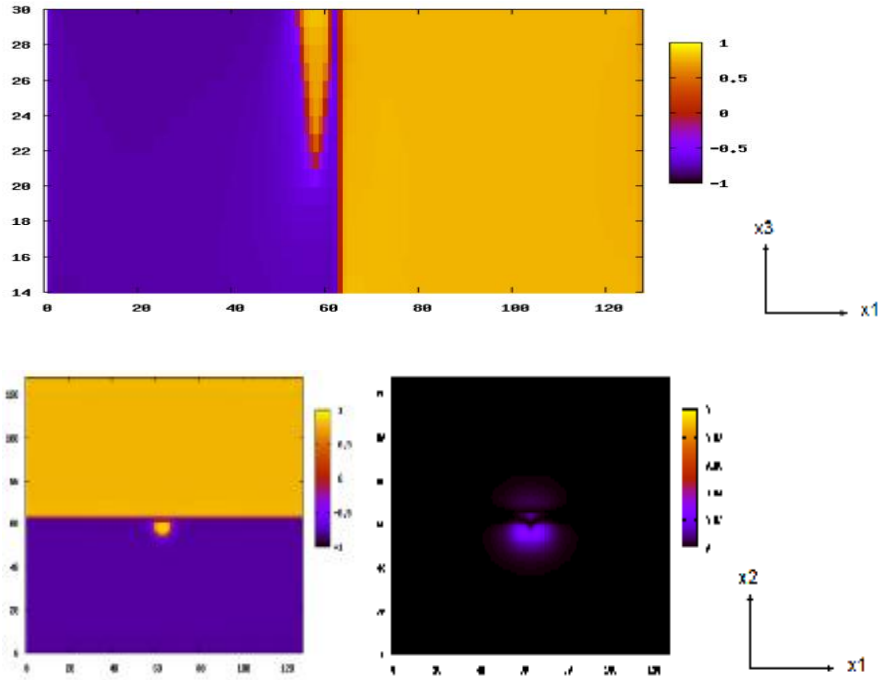

(d)

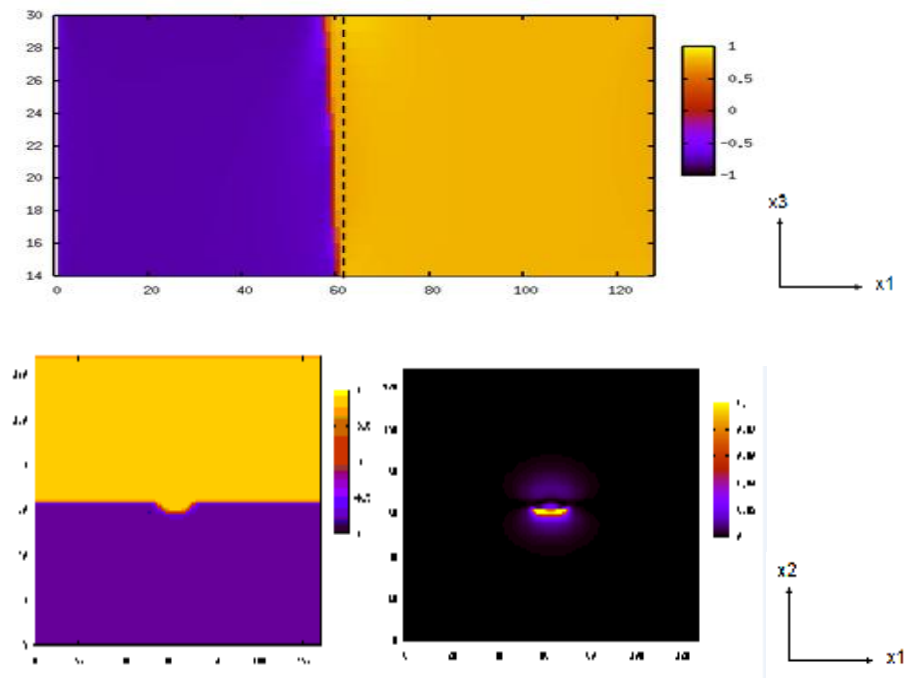

(e)

Fig 3.5 (a) Schematic diagram for the position of the tip and pristine domain structure. (b) Calculated nucleation bias when tip is placed at various positions. Surface projection of out- of -plane polarization

(Unit: 0.7 $\mu C/m^2$) distributions and wall twist (Unit: Arbitrary unit) distribution with a tip bias 7.0V, for various tip positions (c) x_2=40 (d) x_2= 60 (e) x_2=64, respectively

The a-c domain dynamics in PZT has been investigated by many experiments [24, 25].However, the mechanism during domain nucleation and growth has yet been revealed. Inspired by the previous work in $BiFeO_3$ [26], we can reveal the mechanism during twin wall correlated switching.

The pristine domain structure for ferroelastic wall without tip bias is shown in Fig.3 (a), and the electrostatic energy and elastic energy profiles across the domain are given in Fig. 3(c) and Fig.3(d). We can easily see from the profile that the tilt of a-c domain wall is nearly 45°, which will induce asymmetric energy distribution in the two sides of the a-domain. For sake of convenience, we call the left side as "hard side" and right side as "soft side". An energetically active (with respect to electrostatic interactions) region exists near the "soft" (right) side, which would facilitate domain motion under applied fields. In contrast, the "hard" (left) side corresponds to a low energy regime which is largely inactive. The existence of these two regions appears due to elastic interaction: elastic energy distribution show that stress is largely relieved on the left side of the wall (because the wall tilts to the left). In contrast a larger fraction of the c-domain on the right side is under higher compressive stress, leading to higher electrostatic and elastic energies, and hence an increased propensity to become perturbed under applied fields. By contrast, the energy regions of the ferroelectric wall are stable except for the sharp region at the domain wall.

The pristine domain structure for ferroelastic wall without tip bias is shown in Fig.3 (a), and the electrostatic energy and elastic energy profiles across the domain are given in Fig. 3(c)

and Fig.3 (d). We can easily see from the profile that the tilt of a-c domain wall is nearly 45°, which will induce asymmetric energy distribution in the two sides of the a-domain. For sake of convenience, we call the left side as “hard side” and right side as “soft side”. An energetically active (with respect to electrostatic interactions) region exists near the “soft” (right) side, which would facilitate domain motion under applied fields. In contrast, the “hard” (left) side corresponds to a low energy regime which is largely inactive. The existence of these two regions appears due to elastic interaction: elastic energy distribution show that stress is largely relieved on the left side of the wall (because the wall tilts to the left). In contrast a larger fraction of the c-domain on the right side is under higher compressive stress, leading to higher electrostatic and 丁 lower elastic energy, and hence an increased propensity to become perturbed under applied fields. By contrast, the energy regions of the ferroelectric wall are stable except for the sharp region at the domain wall.

When we add tip bias, the nucleation bias profile across a-c domain wall is shown in Fig.3. (d) This result is similar to simulation of Choudbury[16] for PZT (20/80) with a tip half-width 30nm.The nucleation bias is highly reduced in the domain wall neighborhood (to about 1.6 V versus about 2.8 V away from the wall). This confirms that topological defects such as a a-c twin domain wall can be an active nucleation center. We also observe an asymmetrical variation of nucleation profiles. This can be explained by electrostatic energy distribution which originate from the tilt of a domain and the compressive strain and induced charge across the domain wall

Besides, significant differences are shown in Fig.3. (g), with regard to piezoresponse for hard side and soft side. We can see that the most significant enhanced case occurs when tip is placed in 80nm from the point A, which approximately correspond to “soft side” where the electrostatic energy is rather high. The least enhanced case is when the tip is placed 40nm from point A,

which correspond a low-value electrostatic energy region on the surface. These facts indicate when tip placed in various locations the enhancement of piezoresponse is highly dependent on the electrostatic energy on the surface, which is also supported by PFM experiment with band-excitation scanning probe techniques [27].

To further visualize the interaction between tip and ferroelastic wall, we also calculate the wall twist map (the distance between tip and domain wall are 16nm), which is shown in Fig.3 (h). It can be seen that even with a low bias (~0.8V); the wall twist of ferroelastic wall is still significant, compared with that of the ferroelectric wall even with a much bigger bias (Fig.2.(c),(d),(e)). This reflects that ferroelastic domain wall can be highly active with external bias while ferroelectric wall is relatively insensitive. The range of such interaction can reach many ten nanometers while the width ferroelectric wall is less than 10nm. This can roughly explain the fact that even the tip is placed far from the ferroelastic wall, the nucleation bias (~2.8V) is still far less than that of bulk nucleation (~5.2V).

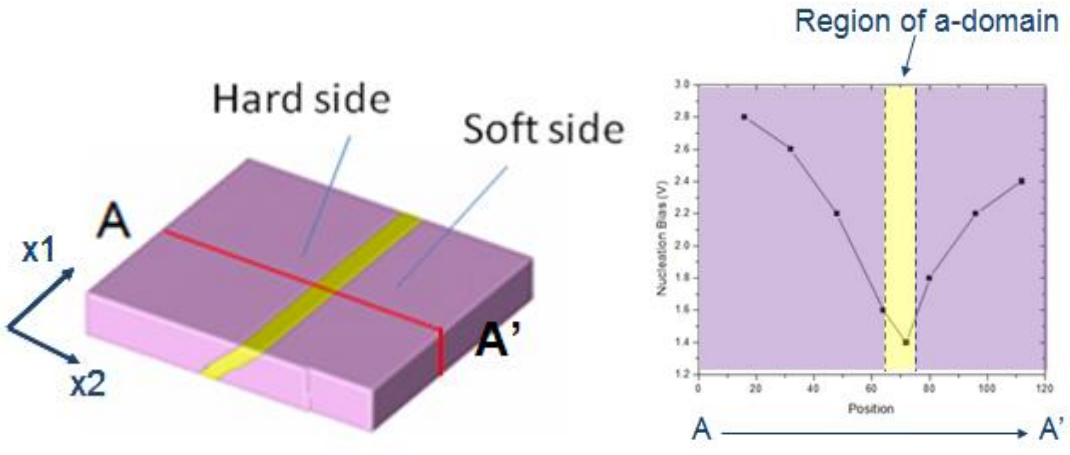

(a) **(b)**

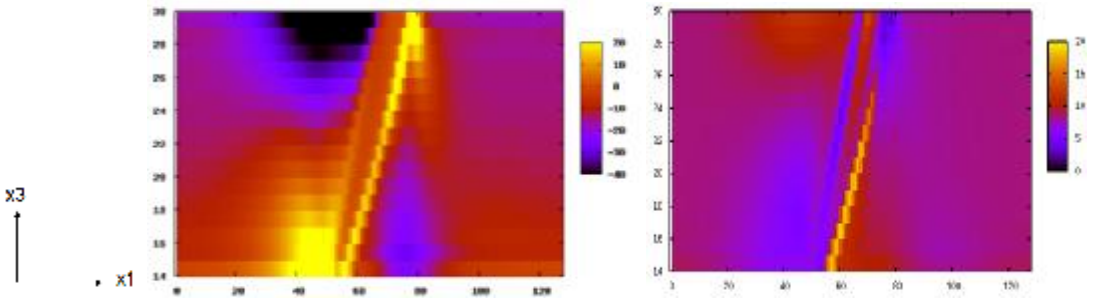
x3
x1

(c) **(d)**

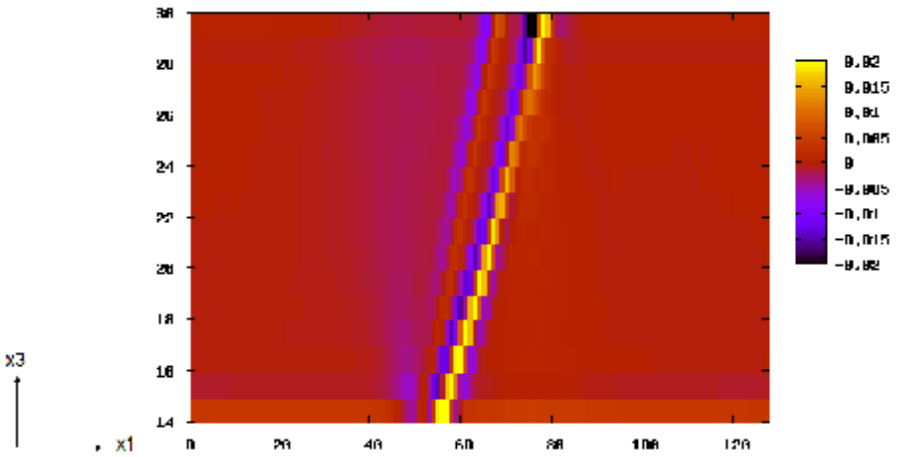
x3
x1

(e)

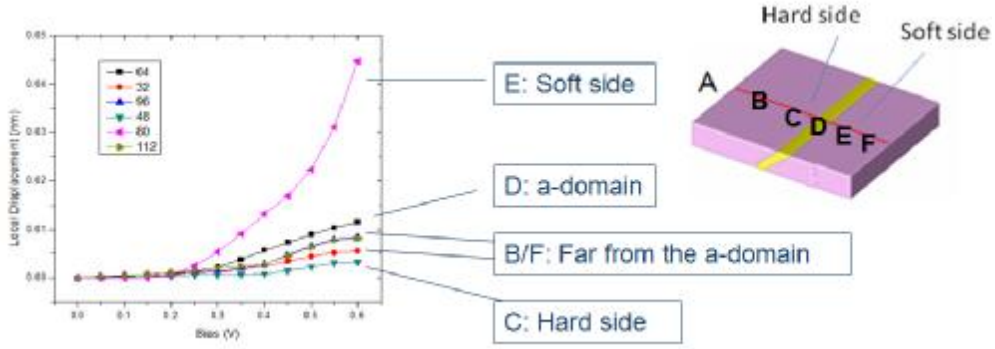
Hard side
Soft side
A
B
C
D
E
F
E: Soft side
D: a-domain
B/F: Far from the a-domain
C: Hard side

(f)

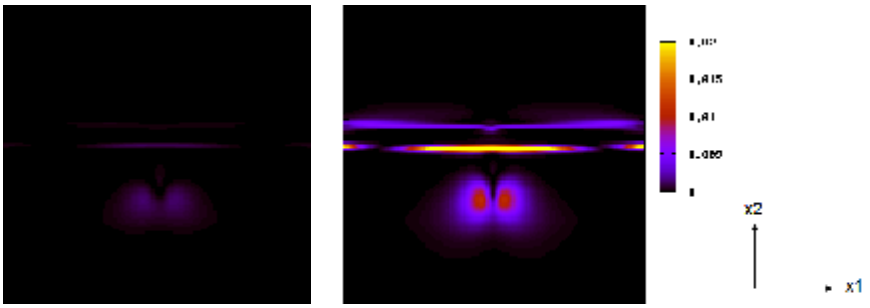

Bias = 0.4 V **Bias = 0.8 V**

（g）

Fig 3.6 (a) Pristine domain structure for PZT thin film with a ferroelastic wall. (b) Nucleation profile across the ferroelastic domain. (c) and (d) Electrostatic energy and elastic energy profile (Unit: J/m^3) across the domain, cutting from x_2-x_3 plane.(e)Bound charge distribution across the domain, cutting from x_2-x_3 plane. (f) Local displacement profile across the domain with sub-nucleation bias (g) wall twist map before nucleation. (The distance between tip and domain wall ~16nm, tip bias = 0.4V and 0.8V)

3.5 Summary

In conclusion, using 3D phase field modeling, we simulate the evolution process of local switching of single domain in PZT ferroelectric thin film, and then include the effect of ferroelectric and ferroelastic domain wall. The difference interaction mechanisms between tip and, ferroelectric wall and ferroelastic wall, respectively are discussed in details, with domain twist, built-in inhomogenity of electrostatic and elastic energy distributions.

References

[1] M. J. Haun, E. Furman, S. J. Jiang, and L. E. Cross, Ferroelectrics. **99**, 13 (1989).

[2] A. L. Kholkin, et.al., MRS Proc. **838E**, O7.6 (2005).

[3] A. Gruverman, O. Auciello, and H. Tokumoto, Appl. Phys. Lett. **69**, 3191 (1996).

[4] S. Jesse. et.al. Nat. Mater. 7, 209 (2008).

[5] N. Balke, S. Choudhury, S. Jesse, M. Huijben, Y. H. Chu, A. P. Baddorf, L. Q. Chen, R. Ramesh & S. V. Kalinin, Nat. Nano. **4**, 868 (2009).

[6] V. Nagarajan, A. Stanishevsky, S.Prasertchoung, T. Zhao, L.Chen, J. Melngailis, A. Roytburd and R. Ramesh, Nat. Mater. **2**, 43 (2003).

[7] Peng Gao, et.al., Adv. Mater. **24**, 591 (2012).

[8] Peng Gao, et.al., Nat. Commun. **2**, 591 (2011).

[9] R. Landauer, J. Appl. Phys. **28**, 227(1957).

[10] M. Molotskii, A. Agronin, P. Urenski, M. Shvebelman, G. Rosenman, and Y. Rosenwaks, Phys. Rev. Lett. **90,** 107601 (2003).

[11] A. N. Morozovska1, Eugene A. Eliseev, Yulan Li, Sergei V. Svechnikov, Peter Maksymovych, V. Y. Shur, V. Gopalan, Long-Qing Chen, and Sergei V. Kalinin, Phys. Rev. B **80**, 214110 (2009).

[12] A. N. Morozovska, Sergei V. Kalinin, Eugene A. Eliseev, V. Gopalan, and Sergei V. Svechnikov, Phys. Rev. B **78**, 125407 (2008).

[13] S. V. Kalinin, B. J. Rodriguez, S. Jesse , Y. H. Chu, T. Zhao, R. Ramesh, S. Choudhury, L. Q. Chen, E. A. Eliseev, and A. N. Morozovska, Proc. Natl. Acad. Sci. **104**, 20204 (2007).

[14] Lun Yang and Kaushik Dayal. J. Appl. Phys. **111**, 014106, (2012).

[15] Aravind, Vasudeva Rao, et.al., Phys. Rev. B **82**, 024111 (2010).

[16] S. Choudhury, J. X. Zhang, Y. L. Li, L. Q. Chen, Q. X. Jia, and S. V. Kalinin, Appl. Phys. Lett. **93**, 3 (2008).

[17] Y. L. Li, S. Choudbury, Z. K. Liu, and L. Q. Chen, Appl. Phys. Lett. **83**, 1608 (2003).

[18] I. A. Kornev, L. Bellaiche, P.-E. Janolin, B. Dkhil, and E. Suard, Phys. Rev. Lett. **97**, 157601 (2006).

[19] S. J. Zhang, C. A. Randall, and T. R. Shrout, J. Appl. Phys. **95**, 4291(2004).

[20] N. A. Pertsev, G. Arlt, A. G. Zembilgotov, Phys. Rev. Lett. **76**, 1364 (1996).

[21] M. J. Haun, PHD Thesis, The Pennsylvania State University, 1988.

[22] L. Q. Chen and J. Shen, Comput. Phys. Commun. **108**, 147 (1998).

[23] Peng Gao, Christopher T. Nelson, Jacob R. Jokisaari, Seung-Hyub Baek, Chung Wung Bark, Yi Zhang, Enge Wang, Darrell G. Schlom, Chang-Beom Eom & Xiaoqing Pan, Nat. Commun. **2**, 591 (2011).

[24] V. Nagarajan, A. Stanishevsky, S.Prasertchoung, T. Zhao, L.Chen, J. Melngailis, A. Roytburd and R. Ramesh, Nat.Mater. **30**, 43 (2003).

[25] Yachin Ivry, Nan Wang, Daping Chu, and Colm Durkan, Phys. Rev. B **81**, 174118 (2010).

[26] Hyejung Chang, et.al., J.Appl.Phys**. 110**, 052014(2011).

[27] R.K. Vasudevan, M.B. Okatan, C. Duan, H. Funakubo, A. Kumar, S. Jesse, L.Q. Chen

S. V. Kalinin, and V. Nagarajan, Adv. Funct. Mater. **22**, 1002(2012)

Chapter 4 Effect of 180 Degree Domain Wall on Local Switching of $BaTiO_3$ Thin Film

4.1 Introduction

Barium titanate or BaTiO3 is the earliest found and still the one of most widely used ferroelectric materials. The BaTiO3 and related materials find many applications by exploiting its dielectric [1], piezoelectric [2], and optical [3] characteristics. For single crystal BaTiO3, the phase transition is complicated. It experiences a para-ferroelectric transition at Curie temperature (125°C), from cubic phase to tetragonal phase. At 8°C, it transforms from tetragonal phase to orthorhombic phase, and finally to rhombohedral phase at -71°C. Coupled with the phase transition, not only the direction of poloarization is changed, but also the lattice constant, and hence a shift of misfit strain for BaTiO3 thin film. Under external load (electrical and mechanical), the domain switching occurs by nucleation of new domain and movement of domain wall, inducing a change of internal stress and electrical field. This will potentially lead to macroscopic failure of ferroelectric materials. Therefore it is necessary to determine the domain switching mechanism with under applied field. Recently, nanodomain was created in a single domain of BaTiO3 thin film, and corresponding domain dynamics was studied by PFM [4]

4.2 Domain Structure of $BaTiO_3$ thin film

Previous experiment by Choi et.al.[5] confirmed the domain structure of $BaTiO_3$ in room temperature can be controlled by the substrate strain. The domain structure will be tetragonal with adequate compressive strain, orthorhombic with adequate tensile strain, and paraelectric between these two cases (Fig.3.1). This result was supported by the calculated results of phase

field approach [6] (Fig.3.1), thermodynamic model [7] and first principle [8]. The domain structures under various substrate-strain conditions was previously obtained by phase-field approach (Fig 3.2)[6].We can see that At room temperature, the domain structure changes from pure tetragonal c domain to c/ a_1/a_2 then a_1/a_2 twin, a mixture of a_1/a_2 twin and O_1/O_2 twin, and then pure O_1/O_2 twin.

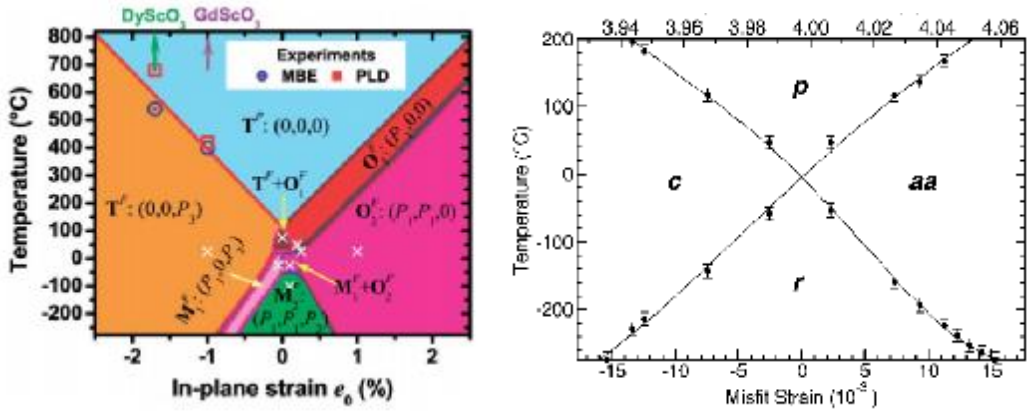

(a) (b)

Fig 4.1 (a) Temperature-strain phase diagram of BaTiO3 calculated by phase-field approach (solid line). The transition temperatures are measured by experiments (scattered symbols). (b) Temperature-strain phase diagram of BaTiO3 calculated by thermodynamics. 'p' represents paraelectric phase, 'c' represents tetragonal phase along x_3 axial, 'aa' stands for orthorhombic phase, and 'r' is monoclinic phase.

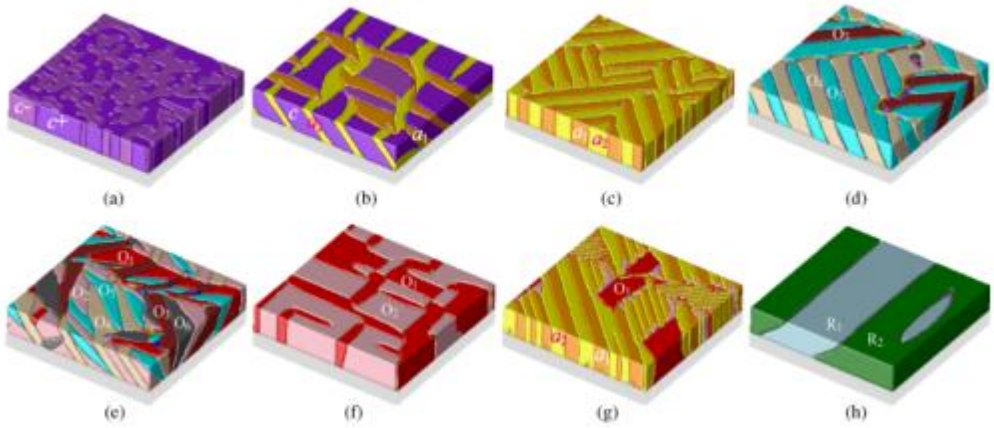

Fig 4.2 Various domain structures of BaTiO3 under various sets of temperature and strain conditions calculated by phase-field approach.

4.3 Calculation Details

The thermodynamics of $BaTiO_3$ can be traced back to the six-order potential written by Devonshire [9]. Later, Bell and Cross [10] modified the first three coefficients to be temperature-dependent. Recently, an eight-order potential was proposed by Li [11] to better describe the phase transition, domain structures and other properties of $BaTiO_3$. Another version of eight-order potential was proposed by Wang [12] with second-order and higher-order coefficients to be temperature-dependent. The values of these four sets of potential are given in Table 4.1 below. It is found Li's potential and Wang's potential are most accurate than Devonshire's version and Cross's version [13]. Here we use Li's for the sake of its simplicity in expression. Corresponding Landau expansion coefficients at room temperature and materials constants are listed in Table 4.2 and Table 4.3. The form of eight-order Landau potential is

$$\begin{aligned} f_{bulk} &= a_1(P_1^2+P_2^2+P_3^2)+a_{11}(P_1^4+P_2^4+P_3^4)+a_{12}(P_1^2P_2^2+P_2^2P_3^2+P_1^2P_3^2) \\ &+a_{111}(P_1^6+P_2^6+P_3^6)+a_{112}[P_1^4(P_2^2+P_3^2)+P_2^4(P_1^2+P_3^2)+P_3^4(P_1^2+P_2^2)]+a_{123}P_1^2P_2^2P_3^2 \\ &+a_{1111}(P_1^8+P_2^8+P_3^8)+a_{1112}[P_1^6(P_2^2+P_3^2)+P_2^6(P_1^2+P_3^2)+P_3^6(P_1^2+P_2^2)] \\ &+a_{1122}(P_1^4P_2^4+P_2^4P_3^4+P_1^2P_3^2)+a_{1123}(P_1^4P_2^2P_3^2+P_2^4P_1^2P_3^2+P_3^4P_1^2P_2^2) \end{aligned} \tag{4.1}$$

Table 4.1 Landau expansion coefficients of BaTiO3. The unit of temperature T is K.

Coefficients	Bell and Cross	Li, et.al.	Wang, et.al.	Unit
a_1	3.34 (T-381)	4.124 (T-388)	3.61 (T-391)	10^5 V m C^{-1}
a_{11}	-2.02	-2.10	-18.3+0.04 T	10^8 V m^5 C^{-3}
a_{12}	3.23	7.97	-22.4+0.067 T	10^8 V m^5 C^{-3}
a_{111}	2.76	1.30	-13.9-0.032 T	10^9 V m^9 C^{-5}
a_{112}	4.47	-1.95	-2.2	10^9 V m^9 C^{-5}
a_{123}	4.91	-2.50	-55.1	10^9 V m^9 C^{-5}
a_{1111}	0	3.86	4.84	10^{10} V m^{13} C^{-7}
a_{1112}	0	2.53	25.3	10^{10} V m^{13} C^{-7}
a_{1122}	0	1.64	28.0	10^{10} V m^{13} C^{-7}

a_{1123}	0	1.37	9.35	10^{10} V m^{13} C^{-7}

Table 4.2 Landau expansion coefficients of $BaTiO_3$ at 300K.

a_1 ($10^9C^{-2}m^{10}N$)	a_{11} ($10^9C^{-4}m^6N$)	a_{12} ($10^9C^{-4}m^6N$)	a_{111} ($10^9C^{-4}m^6N$)	a_{112} ($10^9C^{-4}m^6N$)
-3.63	-2.10	7.97	1.30	-1.95
a_{123} ($10^9C^{-2}m^{10}N$)	a_{1111} ($10^{10}C^{-4}m^6N$)	a_{1111} ($10^{10}C^{-4}m^6N$)	a_{1122} ($10^{10}C^{-4}m^6N$)	a_{1123} ($10^{10}C^{-4}m^6N$)
-2.50	3.86	2.53	1.64	1.37

Table 4.3 Materials constants of $BaTiO_3$ at 300K.

Materials Constants	C_{11} (Gpa)	C_{12} (Gpa)	C_{44} (Gpa)	Q_{11} ($C^{-2}m^4$)	Q_{12} ($C^{-2}m^4$)	Q_{12} ($C^{-2}m^4$)
Values	178	96.4	122	0.010	-0.034	0.029

The time-dependent Ginzburg-Landau equations are solved by semi-implicit Fourier method [14] We used a grid 128 × 128 × 64 with periodic boundary conditions along x_1 and x_2 axes in the film plane. In each direction, the grid spacing is Δx/2, Δx/2, and Δx/4, respectively. The spacing of grid Δx is set as 1nm. The thickness of film is taken as 16 Δx. The gradient energy coefficient is assumed to be $G_{11}/G_{110} = 4.0$ $G_{44}/G_{110} = G_{44}^{'}/G_{110} = 2.0$, where G_{110} is related to Δx by $\Delta x = \sqrt{G_{110}/a_0}$, $a_0 = |a_1|_{T=25°C}$.The substrate strain is chosen as compressive 2% to generate a stable tetragonal domain structure with only c-domains. The temperature used in our simulation is room temperature (300 K). In our simulation, the approximate description of electrical potential applied by a PFM tip with a radius mr0 and location (mx0, my0) is given by

$$f|_{z=0}=0, f|_{z=h}=f_0\frac{mr0}{\sqrt{(x-mx0)^2+(y-my0)^2+mr0^2}} \tag{4.2}$$

4.4 Results and Discussions

To investigate the effect of 180 degree domain wall under inhomogeneous electric field implemented PFM tip, we use a half c+ and half c- stripe domain structure as an example. The pristine domain structure without bias is shown in Fig 4.3. (a). The out-of-plane polarization distribution and displacement distribution along a cross section of x-z plane are also shown in Fig4.3 (b) and (c), respectively. The displacement distribution across the domain wall for various depths into the thin film is given in Fig 4.3 (d). We can see that the effect of 180 degree domain wall on the deformation is mainly on the surface and its effect was easily relaxed by the substrate.

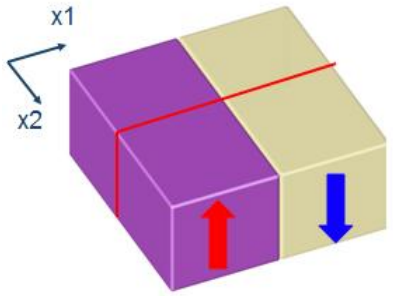

(a)

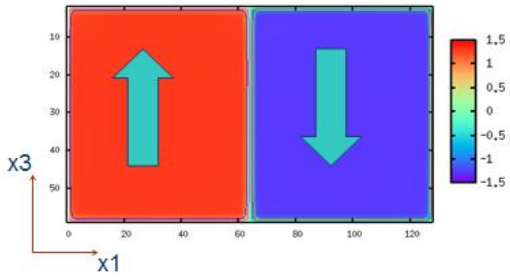

(b)

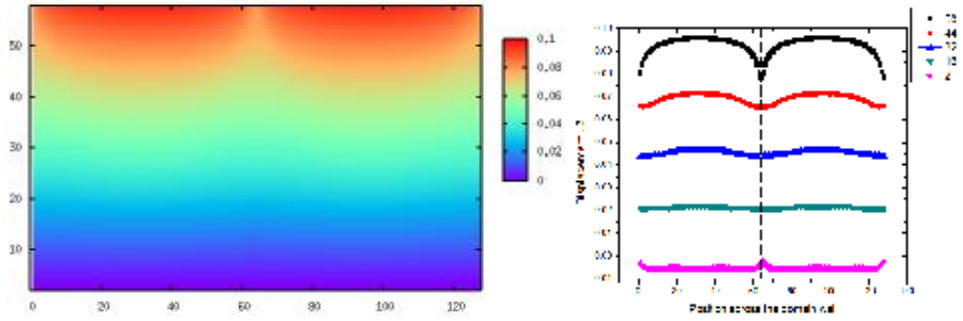

(c)

(d)

Fig 4.3 (a) Schematic diagram of domain structure with180 degree wall (b) The cross-section plot of polarization distribution. (c) The cross-section plot of vertical displacement (u_3) distribution. (d) Distribution of vertical displacement into the thin film with various heights from the substrate.

The tip was placed at various locations on the left side of domain wall in Fig.4.3 (a). A positive voltage was added on the tip in order to induce nucleation of c+ domain. The nucleated bias profile is calculated as shown in Fig 4.4 (a). The trend is qualitatively consistent with phenomenological model [15]. The nucleation bias is very low in region near domain wall and close to that of bulk nucleation when far away from the domain wall. Noticeably, the nucleation bias reaches a small peak in the intermediate region. The rough explanation is illustrated in Fig 4.4 (b). The extra depolarization field (besides the depolarization field of reversal domain) induced by the domain wall charging.

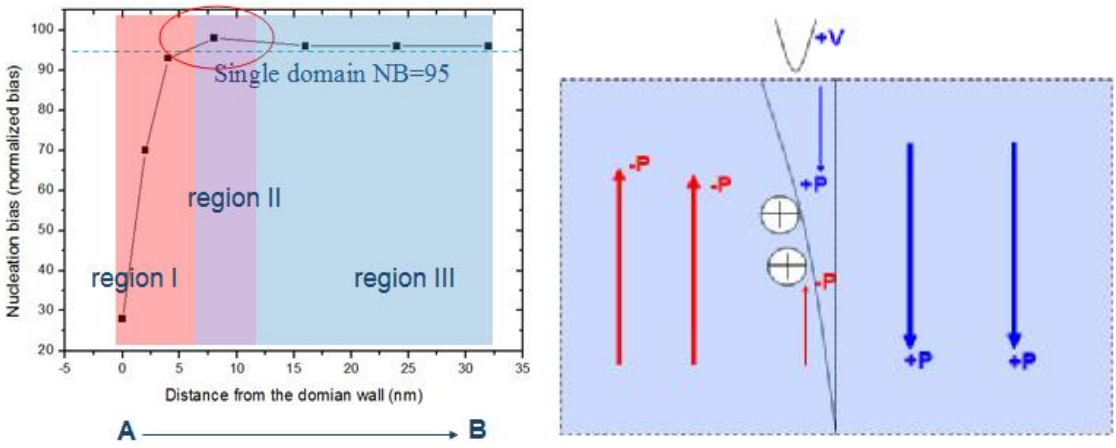

(a) (b)

Fig 4.4 (a) Nucleation bias profile versus distance from the domain wall. (b) Schematic diagram of induced charge and electrical field in our model.

According to Morozokska .et.al. [15], the nucleation mechanism with presence of ferroelectric wall can be categorized into three cases (Fig. 4.6). (i) bulk nucleation, (ii) correlated

nucleation and (iii) domain wall reversible bending. The corresponding nucleation and growth process are shown below. At large tip-wall separation, the mechanism will be bulk nucleation and growth, with tiny long-range effect. The correlated nucleation will occur in the intermediate distance. When tip placed very close or at the wall, the domain bending mechanism will dominate. The nucleation processes for various tip locations are shown in Fig.4.7 for the near region, intermediate region and far region, respectively. Our results are qualitatively consistent with these statements. At large separation between tip and domain wall (region III), the nucleation process is almost the same as that of single domain, e.g., bulk mechanism. If the tip placed on or near the domain wall (region I), the nucleation is mainly due to the bending of nearby c+ domain, leading to very low nucleation bias. With the intermediate tip and domain wall distance (region II), the growth of reversal domain and movement of 180 degree domain wall occurs simultaneously. The growth of domain on the side near the domain wall is inhibited from needle-like, and the nucleation bias is increased due to effect of induced extra depolarization field associated with the ferroelectric wall. This is confirmed by the bound charge distribution with sub-coercive bias (a tip bias a bit lesser than the nucleation bias). As is shown in Fig 4.7, besides the positively charged needle-like region beneath the tip, the bound charge of domain wall on the surface region is largely increased due to attraction of a PFM tip with positive charge and thus, compared with the bulk mechanism, there is an extra depolarization energy inhibiting the formation of reversal c-domain. This analysis would explain the increased nucleation bias in the correlated mechanism (region II).

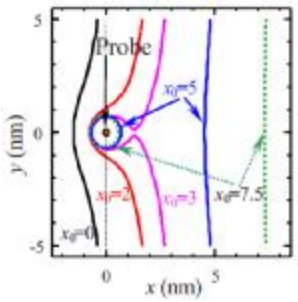

Fig 4.5 Schematic diagram of various nucleation mechanisms (cited from Ref [15,16]). The surface profile of domain wall boundary with various tip positions for $LiNbO_3$ with 180 degree domain wall.

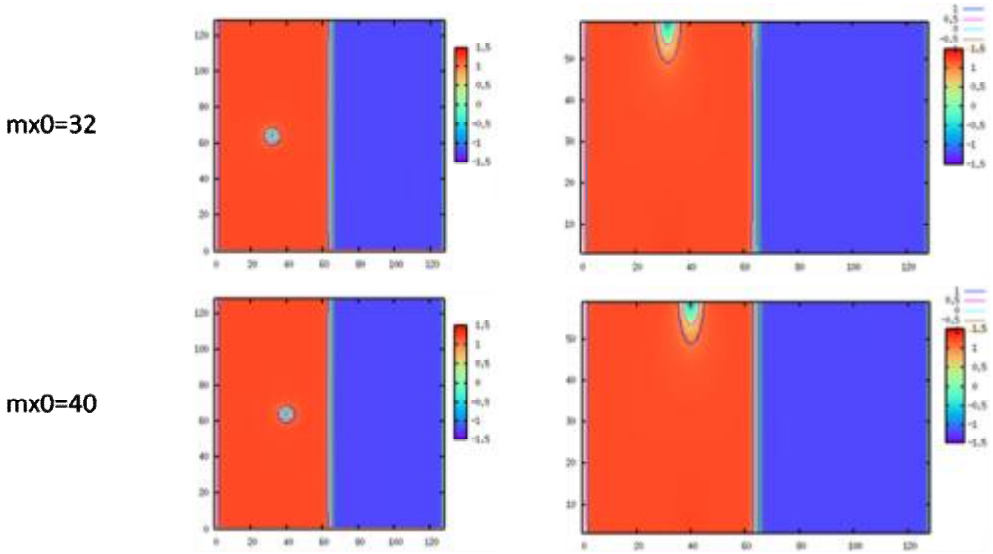

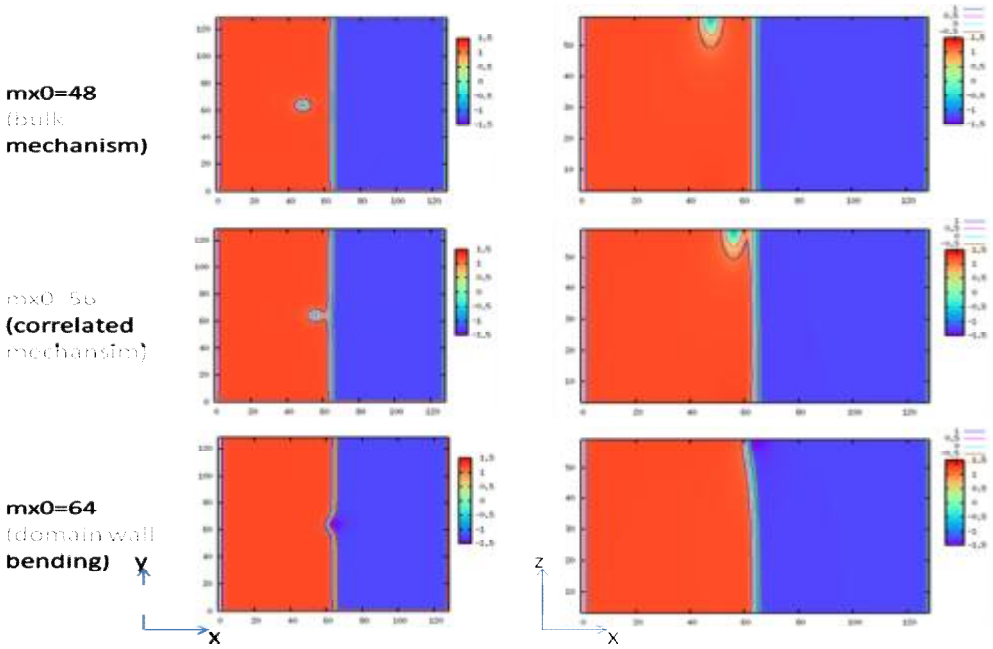

Fig 4.6 Schematic diagrams of nucleation process, with the PFM tip placed at various locations. The color of red to blue corresponds that the out-of-plane polarization varies from to + Ps to – Ps.

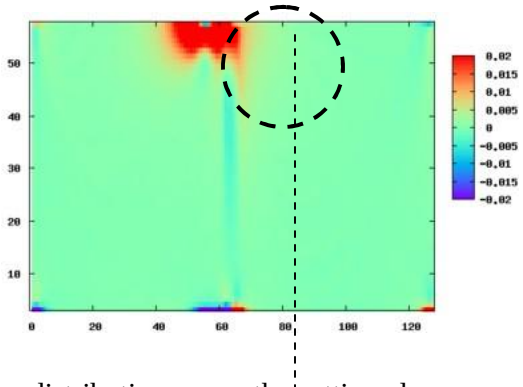

Fig 4.7 Bound charge distribution across the cutting plane x-z, with sub-coercive bias. (Dotted line indicates the position of initial domain wall without bias)

To dig more into the details, we also calculate the surface response displacement profile across the domain wall for different tip locations(Fig 4.8). Under the applied tip bias, the displacement will decrease because the direction of polarization and applied electric field is opposite. For bulk mechanism, the response is symmetrical. For domain bending mechanism, the response is strong in the tip side. For the correlated mechanism, the major decrease is in the left

side of tip, and on the right side the nucleation of reversal domain is inhibited by the domain wall. Specifically, for the domain wall bending mechanism, our results of domain wall response under applied bias is consistent with that of phenomenological model (Fig 4.9).

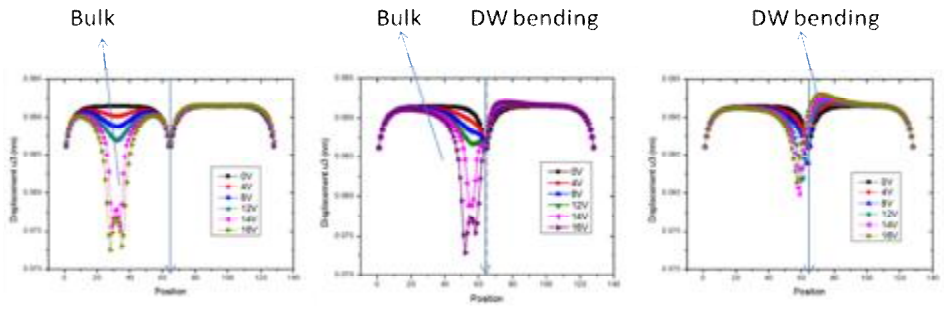

Fig 4.8 The surface displacement across the domain wasll with the increase of tip bias, for three mechanisms, respectively. The blue solid line correspond the position of the domain wall.

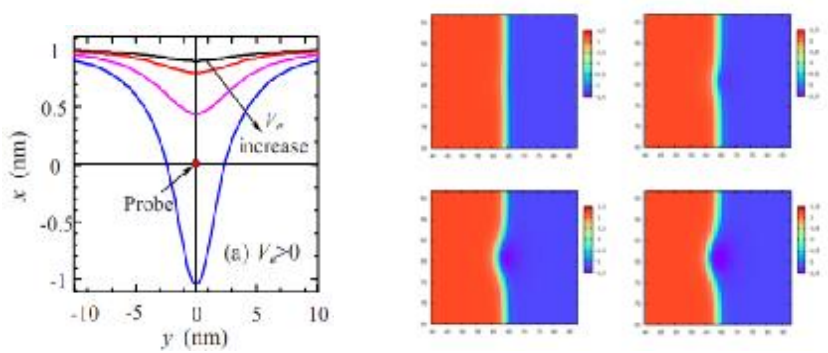

(a) (b)

Fig 4.9 The surface displacement profile along x-y plane with the increase of tip bias, for domain bending mechanisms calculated by (a) phenomenological model [15] (b) our phase-field approach

4.5 Summary

In summary, using 3D phase field modeling, the effect of 180 degree domain wall on local switching of $BaTiO_3$ ferroelectric thin film is investigated. The different interaction mechanisms depending on the distance between tip and 180 degree ferroelectric wall are visualized and discussed in details.

References

[1] A. K. Kingon, J. –P. Maria, and S. K. Streiffer, Nature **406**, 1032 (2000).

[2] D. Czekaj, Z. Surowiak, A. A. Bakirov, and V. P. Dudkievich, J. Eur. Ceram. Soc. **21**, 1609 (2001).

[3] A. Petraru, J. Schubert, M. Schmid, and Ch. Buchal, Appl. Phys. Lett. **81**, 1375 (2001).

[4] N. A. Pertsev,et.al. Nanotech. **19**, 375703 (2008).

[5] K. J. Choi. et.al. Science **306**, 1005 (2004).

[6] Y. L. Li, and L. Q. Chen, Appl. Phys. Lett. **88**, 072905 (2006).

[7] N. A. Pertsev and V. G. Koukhar, Phys. Rev. Lett. **84**, 3722 (2000).

[8] O. Diéguez, S. Tinte, A. Antons, C. Bungaro, J. B. Neaton, Karin M. Rabe, and D.Vanderbilt, Phys. Rev. B **69**, 212101 (2004).

[9] A.F. Devonshire, Adv. Phys. **3**, 85 (1954).

[10] A. J. Bell and L. E. Cross, Ferroelectrics **59**, 197(1984)

[11] Y. L. Li, L. E. Cross and L. Q. Chen, J. Appl. Phys. **98**, 064101 (2005).

[12] Y. L. Wang, A. K. Tagantsev, D. Damjanovic, N. Setter, V. K. Yarmarkin, A. I. Sokolov, and I. A. Lukyanchuk, J. Appl. Phys. **101**, 104115 (2007).

[13] J. J. Wang, P. P. Wu, X. Q. Ma and L. Q. Chen, J. Appl. Phys. **108**, 114105 (2010).

[14] L. Q. Chen and J. Shen, Comput. Phys. Commun. **108**, 147 (1998).

[15] A. N. Morozovska, Sergei V. Kalinin, Eugene A. Eliseev, V. Gopalan, and Sergei V. Svechnikov, Phys. Rev. B **78**, 125407 (2008).

Chapter 5 Mechanical Switching of PZT Thin Film

5.1 Introduction

During the contact process of the PFM tip and a surface in nano-indention not only involves the electrical field but also an inhomogenous stress field is applied on the surface. The domain switching with the presence of mechanical stress has been long studied with a uniform load [1-3]. The polarization rotation caused by simultaneous application of electrical and tip-induced stress has been observed in polycrystalline ferroelectric film [4, 5]. Recently, the local switching of polarization in single crystal ferroelectric thin film by simultaneously electrical and mechanical means was studied experimentally [6]. It is also stated that the flexoelectricity was the major cause. However, further experiments and theoretical studies and phase-field model are needed to validate their results and study the in-depth mechanism.

Our previous phase field models fail to consider the effect of the stress effect especially the surface stress field induced by PFM tip. In this chapter we will first incorporate the surface applied stress load and then investigate the effect of uniform and inhomogenous stress field on a PZT thin film, respectively.

5.2 Calculation details

The applied stress on the surface will only change the mechanical boundary condition.

$$c_{ijkl}\left(\frac{\partial u_k}{\partial x_l} - e_{kl}^{\ 0}\right)\Big|_{x_3=h_f} = s\ (x, y) \tag{5.1}$$

If the size of PFM tip is comparable to the lateral size of thin film, the load on the surface can be approximately viewed as uniform distribution. $s(x, y) = s_0$

If the tip is very slim and the stress load will be highly localized on a small region of contact surface, the stress distribution is also set as Lorentz distribution in our simulation.

$$s(x, y) = s_0 \frac{g^2}{g^2 + (x - x_0)^2 + (y - y_0)^2} \tag{5.2}$$

where j_0 is the center value of tip stress and (x0, y0) are tip coordinates, and γ is the half-width of the tip.

Here, we use a typical tetragonal PZT thin film ($Pb_{0.2}Ti_{0.8}O3$) as an example. Its Landau coefficients and materials constants can be found in Ref [7]. The time-dependent Ginzburg-Landau equations are solved by semi-implicit Fourier method [8].We used a grid 128 Δx × 128 Δx × 36 Δx with periodic boundary conditions along x1 and x2 axes in the film plane. The spacing of grid Δx is set as 1nm. The thickness of film is taken as 20 Δx and 12 Δx for the effective thickness of the substrate layer. The substrate strains for a-c twin wall structure and single c-domain are chosen as compressive 0.5% and 1% respectively. The temperature used in our simulation is 300K.

5.3 Results and Discussions

Firstly, we study the stability of the a-c twin wall structure with the presence of applied surface load. The pristine domain structure without stress is a typical a-c twin wall structure with tilted (approximately 45 degree) [100] a-domain in [001] c-domain matrix. This structure was generated with a compressive substrate strain (0.5%).

Now we applied a uniform positive stress on the surface of thin film (Fig.5.1). We found that a- domain is expanded and stabilized. A positive stress along negative direction of z-axis would induce a 90-degree polarization switching from [001] direction to [100] direction and therefore the volume fraction of a-domain is increased. This is due to the stress direction is anti-paralleled to the polarization direction. It will offset the variant of z-axis, and thus push the internal stress to the outer side of ferroelastic domain wall. If the initial c-domain is along [-100] direction, i.e. paralleled with positive stress, the fraction of c-domain will be increased.

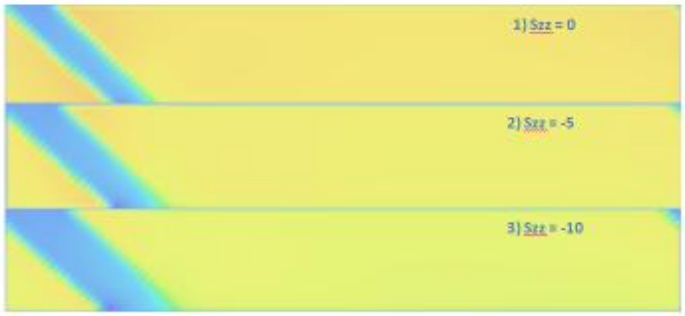

Fig 5.1 The sequential cross section plots of domain structures of PZT (010) plane calculated by phase field modeling. The applied stress szz' applied along the [001] direction (unit 0.25 GPa). The color of sky blue represents *a*-domain, and yellow indicates *c*-domain.

In the presence of an external strain field, the 90-degree switching of PZT thin film occurs once $s_{ij}\Delta e_{ij} + E_i \Delta P_i \geq 2P_s E_c$ [9], where s_{ij} and e_{ij} are the stress and the strain tensors, individually, and E_i and P_i denote the electric field strength and the magnitude of polarization vectors, respectively, P_s and E_c are the spontaneous polarization and the coercive field, respectively. The 90-degree switching could be expected to occur under sufficient strain even in the absence of any external electric field. To examine this speculation, we applied compressive strain along [100] direction. The experimental results, observed in cross sectional tetragonal PZT thin films using in situ transmission electron microscopy (TEM) [10-12] are shown in Fig 5.3(a)

[13]. The phase-field calculations are shown in Fig 5.3 (c). Both results indicated that a compressive shear strain (or stress) can erase a-domain and prefer c-domain. This switching is mainly because of the offset of internal stress of a-c domain wall by the applied compressive strain. The release of internal stress will destabilized the ferroelastic domain wall. It is implied that the erasure of non-180 degree domains should minimize the hindering effect of ferroelastic domains on 180 degree domain wall propagation and increase 180^0 switching volumes, thereby enhancing the piezoresponse.

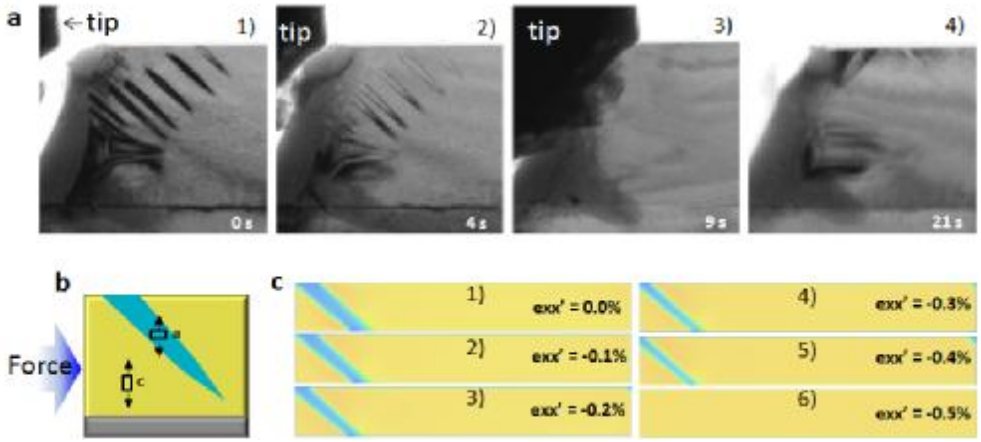

Fig 5.2 (a) Consecutive images showing stress-induced ferroelastic domain erasure[13]. (b) Schematic diagram showing such a stress favors *c*-domain and suppresses *a*-domain, inducing erasure of *a*-domains. (c) The sequential cross section plots of domain structures of PZT (010) plane calculated by phase field modeling. The extra strain ex' applied along the x ([100]) direction, ranges from –0.1% to –0.5%. The color of sky blue represents *a*-domain, and yellow indicates *c*-domain.

Secondly, we investigate the possibility of switching a single c-domain solely with an inhomogenous mechanical load induced by a sharp PFM tip. The pristine domain is a single domain with c-domain along [001] direction and a stress distribution of 2D Lorentz distribution is applied to simulate stress effect of slim tip, as shown in the Fig 5.3. We can see that a reversal c-domain along [00-1] direction is generated and stabilized, with crossed a-domain along [100] and [-100] direction in the vicinity to stabilize the reversal c-domain. The result is similar to the

experiment [6]. However, flexoelectric effect is actually not considered in this calculation. It is still unclear how flexoelectricity can affect this mechanical switching. Further work is needed in this aspect.

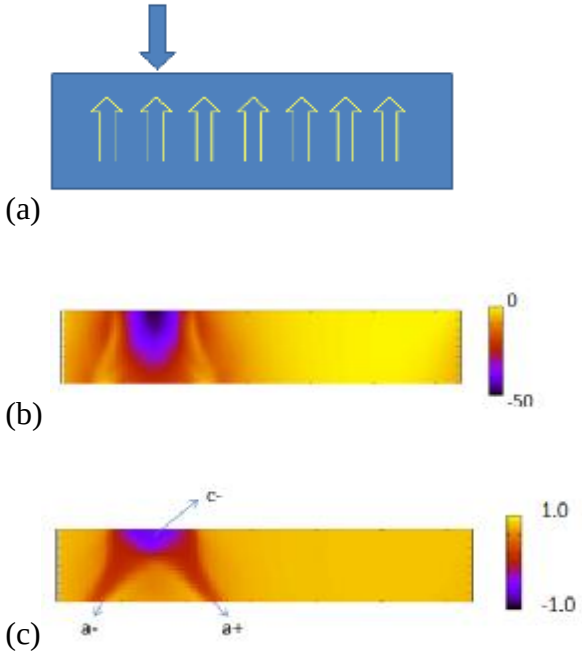

Fig 5.3 (a) Schematic diagram for applying homogenous stress to a single domain with c-domain along [001] direction. (b) Section plot of the stress distribution along the thin film (Unit: 0.025 Gpa). (c) Section plot of the polarization distribution along the thin film (Unit: Spontaenous polarization).

5.4 Summary

In this chapter, applied stress was incorporated into the previous phase-field model to describe the stress effect of PFM tip. For a-c twin walls in PZT thin film under homogeneous applied stress, c-domains are preferred with paralleled pressured positive stress and compressive shear stress while a-domains are preferred with anti-paralleled pressured positive stress and tensile shear stress. Under localized applied stress, the local switching of single domain in PZT thin film is also achieved, which opens the possibility of switching the polarization by mechanical means without any applied electric field.

References

[1] Y. C. Song, A. K. Soh and Y. Ni, J. Phys. D: Appl.Phys**40**, 1175 (2007).

[2] Takahiro Shimada, Yoshitaka Umeno, and Takayuki Kitamura, Phys. Rev. B **77**, 094105 (2008).

[4] C.-T. Sun and A. T. Achuthan, J.Am. Ceram. So. **87**, 395 (2004).

[4] A. Kholkin et.al. Appl. Phys. Lett. **82**, 2127(2003)

[5] A. Gruverman, A. Kholkin, A. Kingon and H. Tokumoto, Appl. Phys. Lett. **78**, 2751(2001)

[6] H. Lu, C. W. Bark, D. Ojos, J. Alcala, C. B. Eom, G. Catalan, A. Gruverman, Science. **336**, 59 (2012).

[7] M. J. Haun, PHD Thesis, The Pennsylvania State University, 1988.

[8] L. Q. Chen and J. Shen, Comput. Phys. Commun. **108**, 147 (1998).

[9] J. Wang, S. Q. Shi, L. Q. Chen, Y. L. Li and T. Y. Zhang, Acta Mater. **52**, 749 (2004).

[10] J. X. Zhang, et.al., Nat. Nano. 6 , 97 (2011).

[11] C. T. Nelson, et. al., Science 334 968 (2011).

[12] H. J. Chang, et.al., J. Appl.Phys. 6, 110 (2011).

[13] P. Gao, et.al.,unpublished.

Chapter 6 Conclusion and Future Works

6.1 Conclusion

In this thesis, a phase-field approach based on Landau theory of ferroelectrics was employed to study the local switching of tetragonal ferroelectrics (PZT, BaTiO3) with considering the effect 180-degree domain wall and 90-degree a-c twinned domain wall in such ferroelectric materials. It is found that under PFM tip bias, effect of such domain walls are distance-dependent and 90-degree domain wall can be favorable for forming of reversal domain and 180-degree domain wall can also be switched. The difference interaction mechanisms between tip and, ferroelectric wall and ferroelastic wall are discussed respectively, with domain twist, built-in inhomogenity of electrostatic and elastic energy distributions. We also preliminarily studied the stability of ferroelastic domain wall with surface stress load, localized or uniform, and found under pressure or compressive shear stress, c domain are preferred.

6.2 Future works

The current works based on phase-field model can be improved by adding the following considerations.

1. The current version of phase-field model for ferroelectrics is not considering the effects of defects. The common point effect in pervoskite oxides is oxygen vacancy which can be important in degradation of ferroelectrics [1]. Also the electron/hole effect should be considered when extending our phase-field model to study the ferroelectric semiconductor heterostructure

and junction. As for line defect, the dislocation can be also integrated into our model [2]. A possible example is to investigate the stability of 90 degree domain wall in PZT under PFM tip bias. Besides, the surface effect associated with Debye screening length has been considered by the phenomenological model of Morozovska [3]. It also can be also incorporated into our phase-field model.

2. In our study the effect of PFM tip are approximately described by a surface potential of Lorentz distribution. However, the real shape of the PFM tip is generally a cone with a constant potential contacted with a small region of the surface of ferroelectrics, with surface bound charge occurs accordingly. Strictly speaking it's an electrostatic boundary problem with irregular boundary problem and it's stricter to get the real potential distribution by finite element modeling and then use it as the input of current phase field model.

3. Current phase field model also neglect the surface stress effect caused by PFM tip. The future phase-field model would consider nano-indention and thus the inhomogenous stress distribution on the surface. Although we have made first step to simulate the mechanical load effect on the domain switching, further phase field study on simultaneous application of electrical field and stress field are needed in future works.

References

[1] D. Kulikov, and Y. Trushin, Ferroelectrics. **308**, 5 (2004).

[2] Y. L. Li, S. Y. Hu, S. Choudhury, M. I. Baskes, A. Saxena, T. Lookman, Q. X. Jia, D. G. Schlom, and L. Q. Chen, J. Appl. Phys. **108**, 10 (2008).

[3] A. N. Morozovska, , and E. A. Eliseev, Phys. Stat. Sol. (b) **8**, 1996 (2006).

[4] H. Lu, C. W. Bark, D. Ojos, J. Alcala, C. B. Eom, G. Catalan, A. Gruverman, Science. **336**, 59 (2012).